Journal of South American Earth Sciences 116 (2022) 103799

Contents lists available at ScienceDirect

Journal of South American Earth Sciences

journal homepage: www.elsevier.com/locate/jsames

Age and provenance of the Mio-Pleistocene sediments from the Sacaco area, Peruvian continental margin

Diana Ochoa [a,*], Thomas J. DeVries [b], Kelly Quispe [c], Angel Barbosa-Espitia [d,e], Rodolfo Salas-Gismondi [a,f], David A. Foster [d], Renzo Gonzales [c], Sidoine Revillon [g], Raul Berrospi [h], Luis Pairazamán [h], Jorge Cardich [a], Alexander Perez [a], Pedro Romero [a], Mario Urbina [f], Matthieu Carré [a,i]

[a] Laboratorios de Investigación y Desarrollo (LID), Centro de Investigación para El Desarrollo Integral y Sostenible (CIDIS), Facultad de Ciencias y Filosofía, Universidad Peruana Cayetano Heredia, Av. Honorio Delgado 430, Lima, Peru
[b] Burke Museum of Natural History and Culture, University of Washington, Seattle, WA, 98195, USA
[c] Programa de Maestría en Ciencias Del Mar, Universidad Peruana Cayetano Heredia, Lima, Peru
[d] Department of Geological Sciences, University of Florida, 241 Williamson Hall, Gainesville, FL, 32611, USA
[e] Instituto de Investigaciones en Estratigrafía (IIES), Universidad de Caldas, Calle 65 # 26-10, Edificio Orlado Sierra, Bloque B, Segundo piso, Manizales, Colombia
[f] Departamento de Paleontología de Vertebrados, Museo de Historia Natural, Universidad Nacional Mayor de San Marcos, Lima, Peru
[g] SEDISOR, LGO-UMR6538, IUEM, Plouzané, France
[h] Escuela de Ingeniería Geológica, Universidad Nacional de Ingeniería, Lima, Peru
[i] LOCEAN-IPSL, Laboratoire D'Océanographie et Du Climat: Expérimentation et Approches Numériques, Sorbonne Université/CNRS/IRD/MNHN, Paris, France

ARTICLE INFO

Keywords:
Peruvian continental margin
Pisco basin
Sacaco
Provenance
U–Pb geochronology
Mio-pleistocene

ABSTRACT

Over the last decades, rocks from the East Pisco Basin (EPB), on the Central Peruvian coast (13°-16°S), have yielded an abundant and diverse collection of coastal-marine fossils, which are key for characterizing the onset and evolution of the modern Humboldt Current. Despite its paleontological richness, and after almost 40 years of study, the spatio-temporal context of the deposits of the southern part of the EPB (Sacaco area) remains only broadly constrained, being mostly tailored to particular vertebrate-rich levels occurring throughout the area.

Here we build a composite stratigraphic section for the Sacaco area including three lithostratigraphic units (Pisco, Caracoles, and Pongo formations), which documents several discontinuities and intraformational unconformities. We infer depositional ages based on new radiometric (U–Pb), isotopic (Sr) and biostratigraphic data, synthesize previous litho-, chemo-, and bio-stratigraphic studies, and present a comprehensive chronostratigraphic review of the Mio-Pleistocene record for the Sacaco sub-basin that allows us to identify various local and basinal events. Our results indicate that, in the Sacaco area, the Pisco Formation ranges from ~9.6 to 4.5 Ma, the overlying Caracoles Formation from 2.7 to ~1.9 Ma, and the Pongo Formation accumulated from ~1.9 up to at least 1.4 Ma. These sedimentary successions accumulated in a continually subsiding setting and show a shallowing-upwards trend. Zircon U–Pb provenance analysis mainly record Neoproterozoic, Cretaceous, and Mio-Pleistocene populations, revealing discrete up-section changes in source areas. Mio-Pleistocene and Cretaceous sources are continuously present, while older recycled-orogen sources vary through time in presence and abundance, indicating either paleogeographic changes or source exhaustion.

1. Introduction

The central Peruvian continental margin has been simultaneously affected by regional Andean uplift and the southeastward migration of the Nazca Ridge (e.g., Hampel, 2002; Horton, 2018). The combined action of these processes has shaped the Neogene-Quaternary evolution of the coastal-marine landscapes and ecosystems. The East Pisco Basin (EPB), located on the central Peruvian margin (13°-16°S and 75°-76°30 W; Fig. 1), contains an extensive sedimentary record that offers an opportunity to understand how different geological and biological processes have affected the continental margin. Despite its long record, the evolution of the EPB continues to puzzle geoscientists. Controversy

* Corresponding author.
E-mail address: diana.ochoa@upch.pe (D. Ochoa).

https://doi.org/10.1016/j.jsames.2022.103799
Received 6 September 2021; Received in revised form 7 March 2022; Accepted 31 March 2022
Available online 6 April 2022

surrounds the southward extension of the EPB and its connectivity with the Sacaco area (S in Fig. 1A), the paleoceanographic conditions of the coastal-marine settings during the warm and permanent El Niño-like phase of the Mio-Pliocene transition (e.g., Fedorov et al., 2006, 2013), the geodynamic factors controlling the evolution of the landscape, and its relationship with the establishment of the coastal desert and the Andes Cordillera uplift (e.g., Garreaud et al., 2010; Rech et al., 2019). To achieve a complete picture of the tectonic, sedimentary, and biological processes acting over the EPB, regional records must be integrated into a reliable chronostratigraphic framework. Over the last decades, the Miocene stratigraphy of the EPB has undergone substantial progress, especially for sedimentary successions from the northern Ica River Valley (e.g., Brand et al., 2011; Di Celma et al., 2016a, 2016b, 2017; DeVries, 2017; DeVries and Jud, 2018; DeVries, 2020; Gariboldi et al., 2017; Bosio et al., 2019, 2020). However, the tectonostratigraphic evolution of the Sacaco area (hereafter referred to as Sacaco sub-basin) remains only broadly known, partly because existing age constraints are limited to scattered fossil-rich stratigraphic levels. Thus, a comprehensive chronostratigraphic model is yet to be defined for the southernmost part of the basin that has yielded most of the latest Miocene-Pleistocene vertebrate fossil record of the EPB.

The record from the Sacaco sub-basin was first described by Steinmann (1904) and Adams (1906, 1908), who associated the fossiliferous Tertiary sedimentary rocks cropping out from Pisco to Chala (13.5°-15.8°S) with the Pisco Formation, ascribing the unit to either the Miocene (Steinmann, 1904) or the Pliocene (Adams, 1908). Since then, the chronostratigraphic framework from the Sacaco sub-basin has relied heavily on morphological trends and evolutionary patterns interpreted from the fossil record (e.g., Lisson, 1925; Steinmann, 1930; Muizon and DeVries, 1985; Muizon et al., 2004; DeVries, 2020). The first absolute ages of the Sacaco's record were obtained from ash layers using radiometric techniques during the 1980s (K–Ar in biotite; Muizon and Bellon, 1980, 1986). Subsequent age refinements of the main fossiliferous localities were provided by Ehret et al. (2012) based on strontium chemostratigraphy, while stratigraphic relations were addressed by Brand et al. (2011) and Lambert and Muizon (2013). Recently, DeVries (2020) reviewed the litho- and molluscan biostratigraphic record of the Sacaco sub-basin and proposed a subdivision of the Neogene-Quaternary stratigraphic sequences, defining two new lithostratigraphic units (Caracoles and Pongo formations; Fig. 2). Furthermore, U–Pb radiometric ages for upper Pisco sedimentary rocks and the lower Caracoles Formation were provided by Ochoa et al. (2021). A robust chronostratigraphic framework is, however, still needed for various vertebrate-bearing successions ascribed to the Pisco Formation and the recently defined Caracoles and Pongo formations, so that the spatio-temporal context of the fossiliferous content can be properly assessed.

Herein, we present new age constraints, review and update the Mio-Pleistocene stratigraphic framework of the Sacaco sub-basin, including the Pisco, Caracoles, and Pongo formations. To achieve this goal, the stratigraphic record from ten localities across the Sacaco sub-basin was described and sampled for radiometric (U–Pb), isotopic (Sr/Sr), or biostratigraphic purposes. The integrated chronostratigraphic framework was then used for exploring the evolution of the Sacaco sub-basin

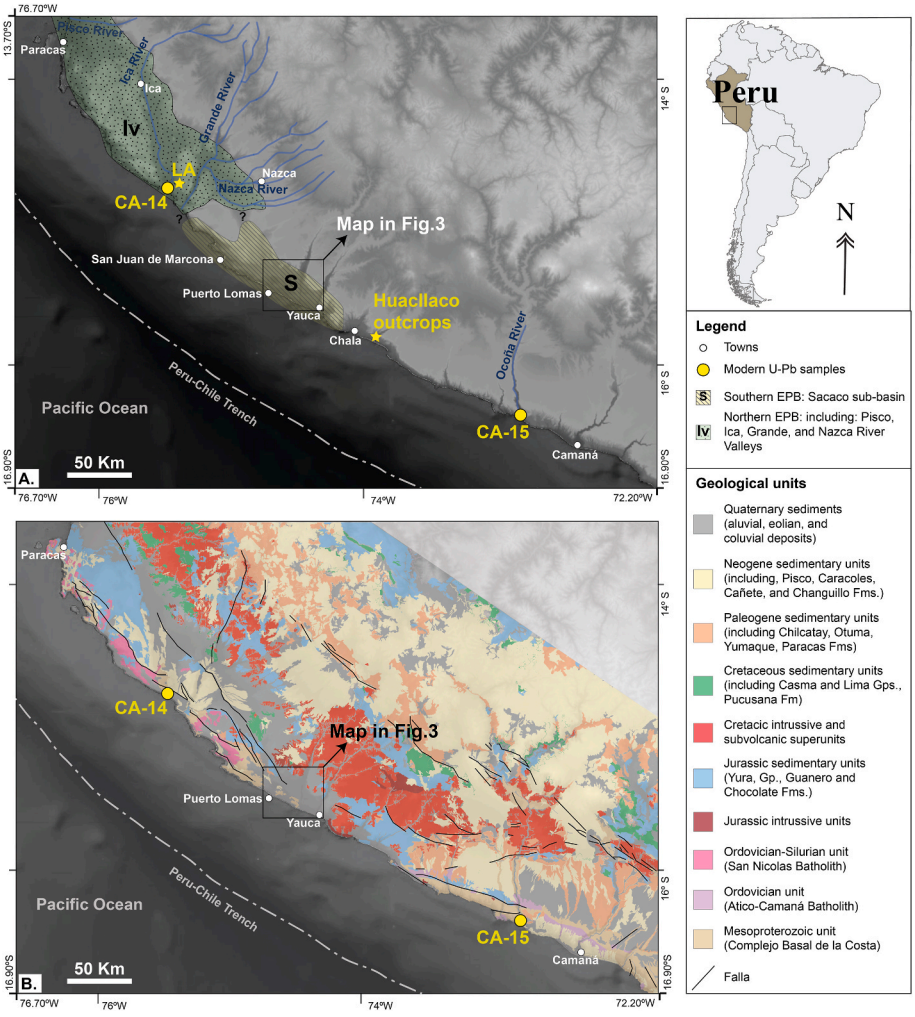

Fig. 1. A). Location map of the East Pisco Basin (EPB), showing extension of the northern (Iv) and southern (S) EPB. LA: Laberinto Area. Main river valleys associated with the northern EPB are shown in blue (data derived from HydroSHEDS). **B).** Simplified geologic map of the Central Peru region (12°-17° S, 70°-78°W; modified from INGEMMET, 2016, 2017). Yellow dots indicate modern U–Pb samples from the Ica (CA-14) and Ocoña Rivers (CA-15) used to compare distribution of detrital zircon-ages (data from Pepper et al., 2016).

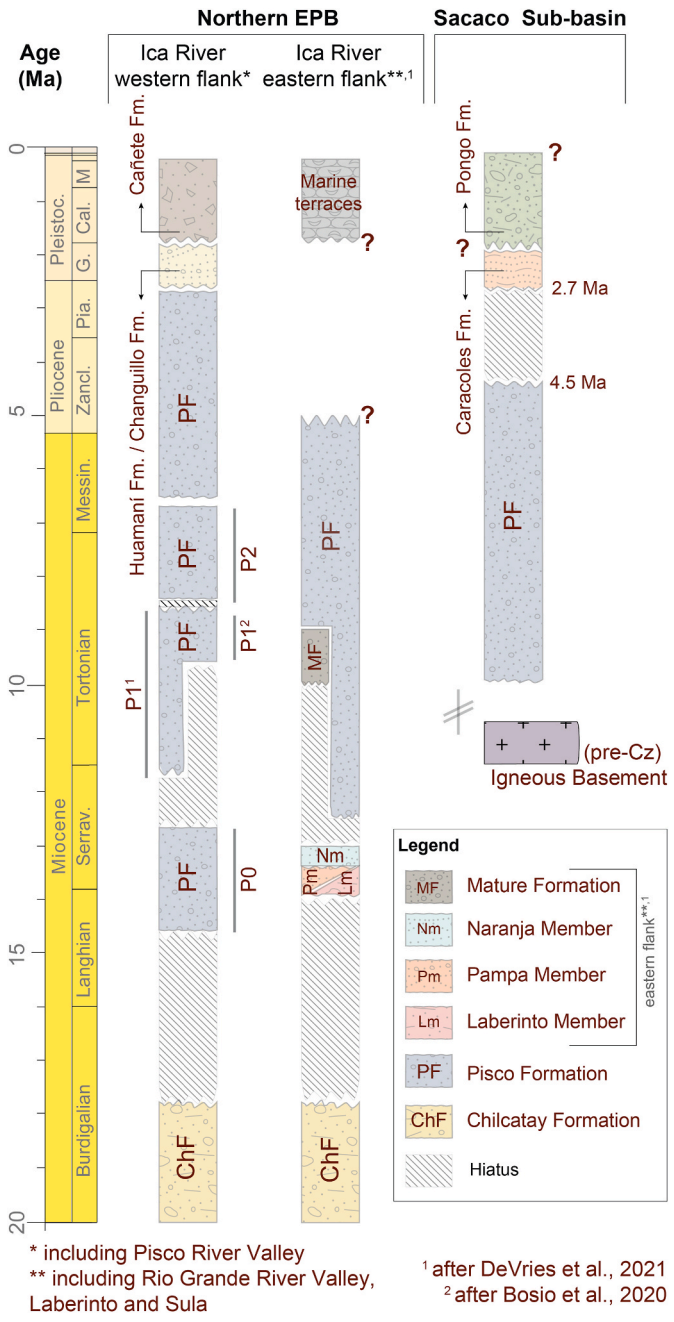

Fig. 2. Existing chronostratigraphic frameworks for Neogene sediments from the Ica River Valley (western and eastern flanks) and the Sacaco sub-basin. Northern EPB age constraints after Bosio et al. (2019, 2020); DeVries and Jud (2018; 2020); DeVries and Jud (2018); Di Celma et al. (2016a; 2016b, 2017, 2018). Sacaco sub-basin age constraints after Muizon and DeVries (1985); Ehret et al. (2012); and Ochoa et al. (2021). Note that ages of the Chilcatay Fm are under debate (see DeVries et al., 2021).

and its relation with the northern EPB (Ica and Pisco valleys). Furthermore, we studied the U–Pb zircon age distribution of a suite of samples from various sedimentary successions from the Sacaco sub-basin to carry out a sediment provenance analysis.

2. Geological setting

The EPB is an elongated forearc basin located on the Peruvian continental margin (13°-16°S and 75°-76°30 W; Fig. 1). The basin is bounded landwards by the Coastal Batholith and towards the ocean (westwards) by the Coastal Cordillera. The EPB became a sedimentary trap during the Eocene, in response to the eastward subduction of the Nazca plate below the South American margin (Macharé and Ortlieb, 1992; León et al., 2008). Sedimentary and stratigraphic architecture indicate the presence of at least two active depocenters since the late Miocene (about 11 Ma; Dunbar et al., 1990). These depocenters are physically separated by topographic highs, formed by Paleozoic and Mesozoic rocks from the San Nicolas Batholith and the Coastal Batholith, respectively (Fig. 1). The northern depocenter (herein referred to as the northern EPB) includes the Pisco, Ica, and Grande River Valleys (Iv in Fig. 1A), and corresponds to the largest and deepest accumulation zone where medium-grain sandstones and diatom-rich deposits have predominated since Eocene times (e.g., Dunbar et al., 1990; León et al., 2008; Di Celma et al., 2016a, 2016b). Whether the Nazca River Valley was also connected to the northern and/or southern depocenters remains to be investigated. The southern depocenter corresponds to the Sacaco sub-basin, a smaller accumulation area receiving mainly sand-sized clastic sediments since the late Miocene (Fig. 1A). Both areas of sediment accumulation contain frequent ash and sandy-ash layers associated with Neogene Andean volcanism.

We focus here on the Mio-Pleistocene sedimentary successions cropping out in the Sacaco sub-basin, including the Pisco Formation (Caldas, 1978; Macharé, 1987), as well as the recently described Caracoles and Pongo formations (DeVries, 2020, Fig. 2). The Pisco Formation, the oldest unit of the three, is the only one that (discontinuously) extends over the entire EPB (Adams, 1908; Caldas, 1978). It is known by its well-preserved and diverse fossiliferous content (e.g., Adams, 1908; Lisson, 1925; Colbert, 1944; Caldas, 1978; Macharé, 1987; Muizon and DeVries, 1985; Ehret et al., 2012; Lambert and Muizon, 2013; DeVries and Jud, 2018; 2021) and is interpreted to represent open to protected coastal to shallow-marine settings across the shoreface and offshore shelf (e.g., Marocco and Muizon, 1988; Dunbar et al., 1990; Di Celma et al., 2016a, 2016b). In the northern EPB, the Pisco Formation was deposited from the middle Miocene to the Pliocene (14.8 to ?2.5 Ma; Macharé and Fourtanier, 1987; Solis, 2018; Bosio et al., 2020), whereas in the southern EPB the unit only spans the late Miocene to early Pliocene (~10–4.5 Ma; Muizon and Bellon, 1986; Ochoa et al., 2021, Fig. 2). To date, in the northern EPB, three intraformational unconformity-bounded transgressive sequences have been recognized on Miocene successions from the western flank of the Ica River (Fig. 2; Di Celma et al., 2017, 2018; Bosio et al., 2020). These are defined, from oldest to youngest, as: P0 (14.8–12.4 Ma), P1 (starting either from 12.5 Ma [DeVries and Jud, 2018; 2021] or 9.5 Ma [Di Celma et al., 2017, 2018; Bosio et al., 2020] up to 8.6 Ma), and P2 (8.6-at least 6.7 Ma). By contrast, along the eastern flank (Laberinto area; LA in Fig. 1), five lithostratigraphic units (undifferentiated Pisco, Laberinto, Pampa, and Naranja members of the Pisco Formation, and Mature Formation; Fig. 2), which are correlative with the P0 and P1 allomembers, have been described (DeVries and Jud, 2018; DeVries et al., 2021). Similar sequence-stratigraphic architectures have not been identified in the southern EPB.

In the Sacaco sub-basin, the Pisco Formation is unconformably overlain by the Caracoles Formation, which reach up to 50 m in thickness. The Caracoles Formation consists of green olive to brown, mottled medium-grained massive and bioturbated sandstones, interbedded with indurated coquina beds containing bivalves (e.g., *Mulinia, Pitar, Amiantis domeykoana, Eurhomalea fuenzalida*, among others), gastropods (e.g., *Crepipatella dilatata*, *Nassarius*), and barnacles (DeVries, 2020; Ochoa et al., 2021). The unit is interpreted as accumulated in shallow marine settings, likely a (semi-) restricted embayment during Plio-Pleistocene times (DeVries, 2020). The base of the unit was dated at 2.7 Ma (Fig. 2, Ochoa et al., 2021), while a precise age for the uppermost part of the Caracoles unit has yet to be obtained.

The youngest marine unit, excluding the middle-late Pleistocene marine terraces (e.g., the Totoral Tablazo of DeVries, 2020; Macharé and Ortlieb, 1992), corresponds to the Pongo Formation. DeVries (2020)

describes this unit as consisting of up to 60 m of poorly consolidated to unconsolidated coarse-grained sands, rounded pebbles and cobbles of crystalline basement rocks, including frequent shell banks and lenses, disperse invertebrate fragments (mollusks, gastropods, and cirripeds), and bioclastic debris. An intraformational unconformity separates the Pongo Formation into two distinct allosequences (DeVries, 2020). The lower one is dominated by poorly consolidated green to brown massive coarse-grained sands (Pongo-1), while the upper sequence is mainly composed of unconsolidated coarse-grained gray to brown bioclastic sands, pebbles, cobbles (Pongo-2). The lag surface associated with this intraformational unconformity can be recognized by the first occurrences of *Argopecten purpuratus* (DeVries, 2020). Sedimentary rocks from the Pongo Formation are considered to be accumulated along high-energy sandy beaches. No absolute dates are available for the Pongo Formation; however, the unit is considered either as early Pleistocene (circa 2.5 Ma; scenario 1 of DeVries, 2020) or as latest early Pleistocene (1.2–0.9 Ma) based on its stratigraphic position and malacological fauna (scenarios 2 and 3 of DeVries, 2020).

3. Materials and methods

3.1. Field data

The Mio-Pleistocene outcrops of the Sacaco sub-basin consist of (mostly) sub-horizontal shallow marine to coastal deposits (Marocco and Muizon, 1988; DeVries, 2020) that occur as disconnected patches and are often covered by recent eolian sand deposits. It is thus necessary to integrate multiple stratigraphic sections to have a robust chronostratigraphic framework for reconstructing the geological evolution of the sub-basin. Hence, we built a composite section integrating the rock record from ten localities spread cross an area of ~250 km^2 (Fig. 3). Studied sections include those described by Muizon and DeVries (1985; Aguada de Lomas, Montemar, Sacaco Chacra in Fig. 3) and the type sections defining the Caracoles and Pongo units (DeVries, 2020; Quebrada Caracoles and Quebrada Pongo in Fig. 3), as well as newly visited exposures. All geologic sections were measured using a Jacob staff and a Brunton compass. Despite the low dips and the rare occurrence of conspicuous marker beds, it was possible to establish the stratigraphic position of individual localities within the Mio-Pliocene sequence thanks to the regional SE dipping trend. Appendix A includes a GPS list of main observation points, sampling sites, as well as detailed stratigraphic columns for each of the visited localities. Following previous notation styles (Muizon and DeVries, 1985; Lambert and Muizon, 2013), we refer to localities by using full names whereas abbreviations are exclusively used for vertebrate-bearing levels. Note that our composite section is built from observations associated with rock localities instead of isolated vertebrate-bearing levels. From oldest to youngest, the reviewed localities include: Aguada de Lomas, Yauca Road Cut, Montemar, Sud-Sacaco West, the renowned Sacaco (hereafter referred to as Sacaco Chacra), Yauca Depressions, Cerro Amarillo, Quebrada Caracoles, and Quebrada Pongo (Fig. 3).

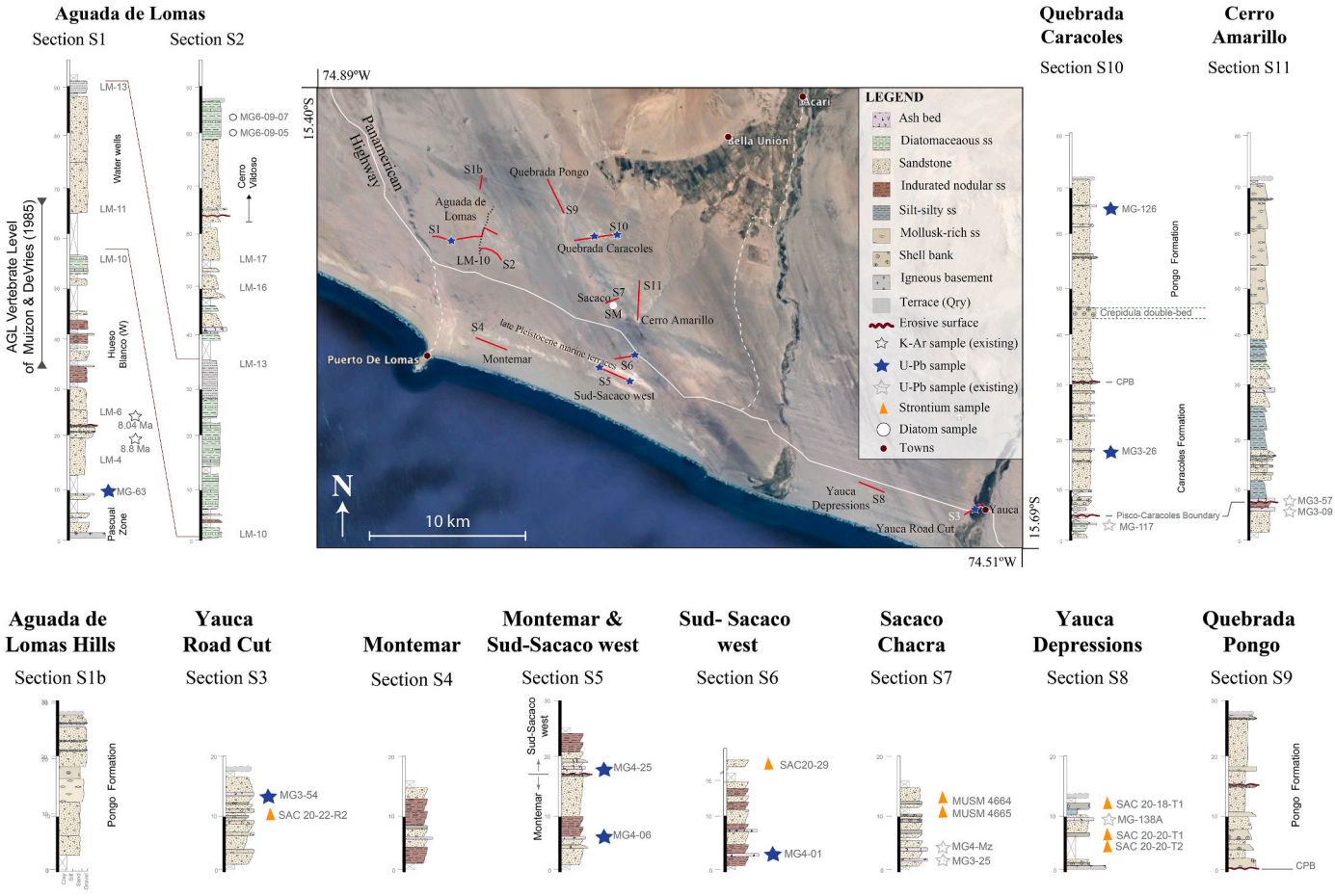

Fig. 3. Map of the Sacaco area and stratigraphic logs from the Pisco, Caracoles, and Pongo formations cropping out at Aguada de Lomas (sections S1, S1b, S2), Yauca Road Cut (section S3), Montemar (sections S4 and S5), Sud-Sacaco West (section S6), Sacaco Chacra (section S7), Yauca Depressions (section S8), Quebrada Pongo (section S9), Quebrada Caracoles (section S10), and Cerro Amarillo localities (section S11). Guide beds (LM) proposed by Brand et al. (2011). Blue filled stars: U–Pb ages after this study. Black filled stars: existing U–Pb ages. SM: Sacaco Paleontological Museum. CPB: Caracoles-Pongo Boundary. Qry: Quaternary. Satellite imagery from SAS. Planet (GPLv3).

3.2. U–Pb geochronology

3.2.1. Maximum depositional ages

Seven tuffs and ashy sandstones were collected across the Sacaco sub-basin, from the Pisco (n = 5; MG-63; MG3-54; MG4-6; MG4-25; MG4-01), Caracoles (n = 1; MG3-26), and Pongo formations (n = 1; MG-126), for determining U–Pb maximum depositional ages and provenance constrains (Table 1). Analyses were carried out at the Department of Geological Sciences of the University of Florida. Zircon crystals were isolated from a 2-kg sample using standard procedures, including rock disaggregation and gravimetric and magnetic separation techniques. Only euhedral, colorless grains lacking visible inclusions were chosen for analysis. In all samples, a minimum population of 40 zircon crystals was analyzed and ages were determined based on the youngest $^{206}Pb/^{238}U$ weighted mean ages of at least three crystals. In the case of the Yauca Road Cut (sample MG3-54) and the Sud-Sacaco West (samples MG4-25 and MG4-01) localities, maximum depositional ages were estimated using only the youngest single grain (Table 1). Maximum depositional ages are reported with standard error uncertainties at 2σ and 95% confidence intervals (Table 1; Fig. 4). The IsoplotR package (Vermeesch, 2018) from the open-source R program (R-Core Team, 2018) was used to calculate the weighted mean age. Zircon weighted mean ages per sample are shown in Fig. 4. Isotopic values obtained for zircon grains from two U–Pb samples reported by Ehret et al. (2012) for El Jahuay (Alto Grande) and Sud-Sacaco West were also reinterpreted following the same procedure as noted above (Appendix B). Further details on geochemical analysis and complete data on zircon U–Pb age determinations are given in Appendix B.

3.2.2. Zircon age distributions and provenance analysis

Zircon-age distributions were evaluated to assess changes in sediments source in the Sacaco sub-basin during the last 10 My (Fig. 5; Appendix B). For this, we compared the detrital ages from the Sacaco sub-basin with bedrock and modern-river derived zircon-ages. We compiled a dataset with 861 U–Pb zircon ages. Of these, 686 correspond to U–Pb zircon ages from different Mio-Pleistocene strata across the sub-basin, including our results and those reported by Ehret et al. (2012) and Ochoa et al. (2021). The remaining 175 are zircon ages derived from two modern rivers draining across the region reported by Pepper et al. (2016). One modern sample comes from the Ica River, which runs through the northern EPB (CA-014 in Fig. 1A, n = 78), the other from an extrabasinal stream, the Ocoña River (CA-015 in Fig. 1A, n = 97), located about 150 km to the south of the EPB's southern margin. To date, we have no detrital modern river samples from watercourses draining across the southern EPB. The extrabasinal detrital sample was chosen because its valley reached its present-day level by the early Pliocene (Thouret et al., 2007) and it drains within a catchment area that includes similar bedrock (the Coastal Batholith, the San Nicolas Batholith, the Arequipa Massif, and the Eastern Cordillera) as occurs in catchment areas of the Sacaco sub-basin (Fig. 1A). Zircon-ages were then compared against published U–Pb zircon ages from bedrock that could have served as sediment sources for the central Peruvian Pacific margin (Pepper et al., 2016), such as the Coastal Batholith (e.g., Mukasa, 1986; Wipf, 2006), the San Nicolas Batholith (e.g., Ramos, 2008), the Arequipa Massif (e.g., Loewy et al., 2004; Chew et al., 2008), the Eastern Cordillera (e.g., Mišković et al., 2005), or recycled from the Amazon Craton (e.g., Cardona et al., 2009).

3.3. Strontium-based chronology

Seven shark teeth samples (Sud-Sacaco West [n = 2], Sacaco Chacra [n = 2], and Yauca Depressions localities [n = 3]) and one aragonitic $CaCO_3$ sample (Yauca Road Cut [n = 1]) were analyzed for Sr radiogenic isotopes (Table 1). About 5–10 mg per sample were weighted and dissolved in savillex beakers in ultra-pure acetic acid 30% for 24 h at 100 °C on a hot plate. After evaporation to dryness, dry residues were taken up into 1 ml of ultra-pure HNO_3 1 M and centrifuged before loading on Biorad® columns using Eichrom® Sr-SPEC resin (Pin and Santos-Zalduegui, 1997). Sr was eluted in 2 ml of hot ultrapure H_2O. Procedural blanks were all below 200 pg so negligible in all cases. Samples were loaded on W filaments and Sr isotope compositions were measured in static mode on a Thermo TRITON at the Pôle de Spectrométrie Océan from the Ocean Geosciences Laboratory (Brest, France). All measured Sr ratios were normalized to $^{86}Sr/^{88}Sr = 0.1194$. During the course of analysis, Sr isotope compositions of standard solution NBS987 gave $^{87}Sr/^{86}Sr = 0.710275 \pm 0.000008$ (2σ, n = 6, recommended value 0.710250). Strontium isotope ratios measured from the Pisco Formation are shown in Appendix C. Measured ratios were converted to age values using the LOWESS dataset (V5; Fit 26/03/13; McArthur et al., 2012). Mean age corresponds to the mean isotopic ratio on the mean age-ratio curve, while the youngest and oldest ages correspond to the mean ±2σ on the lower and upper curves, respectively.

4. Results

4.1. A composite stratigraphic record for the Sacaco sub-basin

Aguada de Lomas: This locality occurs 2 km off the Panamerican Highway and about 10 km east of the Puerto Lomas village (Fig. 3). Sedimentary successions from the Aguada de Lomas locality are well-known for their fossiliferous content (e.g., Muizon et al., 2003; Pilleri and Siber, 1989; Brand et al., 2011). The stratigraphic record from this locality was formerly addressed by Muizon and DeVries (1985), and in greater detail by Brand et al. (2011). The locality includes the AGL vertebrate level of Muizon and DeVries (1985). The rock succession herein presented consists of two sections that are referenced to five well-known local landmarks (Appendix A). At this locality, the Pisco and Pongo formations are observed. Clastic Pisco sediments unconformably overlie igneous rocks from the San Nicolas Batholith, and Pongo sediments unconformably overlie those of the Pisco Formation. An approximate thickness of 140 m was calculated with triangulation for the Pisco Formation, using an average dip direction/dip angle of 102°/7°. The succession consists of alternations of gray and yellow sandstones that locally become hard-grounds. Sandstones vary in grain sizes (from fine-to coarse-grained), sorting, and degree of cementation. Sandstone beds are often bioturbated and show parallel lamination. Centimeter-thick shell banks, diatomite, and chert beds also occur locally throughout the succession (Fig. 3). Two well-developed conglomeratic beds occur towards the base of the succession (21 and 23 m from the base of the Section S1; Fig. 3), topped by an angular unconformity. The sedimentary section continues with meter-thick massive to slightly-laminated sandstone beds that intercalate with shell banks, indurated gray sandstones, and tuffaceous and diatomaceous sands. Towards the top (at Cerro Vildoso), shell banks and lenses become frequent, and bioturbation intensity decreases (Appendix A). A centimeter-thick ash level close to the base of the succession was sampled for radiometric dating (MG-63; Fig. 3). Additionally, two samples were taken in the uppermost levels of the succession for biostratigraphic purposes (MG6-09-05 and MG6-09-07; Fig. 3). The Pongo Formation crops out to the east, as part of the hills enclosing the locality (section S1b in Fig. 3). The Pongo succession is dominated by gray to olive medium-to-coarse immature sandstones intercalating with pebbly-cobbly conglomerates, and common occurrences of mollusks shells, shark teeth and vertebrate remains (including penguins and pinnipeds [MUSM 3624]; section S1b in Fig. 3).

Yauca Road Cut: This locality encompasses a continuous rock exposure from the Pisco Formation occurring along the Panamerican Highway, about 1.5 km southwest of the Yauca village (Fig. 3). The entire section is less than 20 m thick and is composed of intercalations of yellowish sandstones, polymictic conglomerates, and shell banks dominated by *Anadara chilensis* (see Section S3 in Fig. 3). Sandstone beds are massive to laminated with bioturbation, lack clear grading, and

Table 1
Geographic and stratigraphic position of existing age constraints for the Sacaco Sub-basin. Gray bands show data provided in this study. References as follows: (1) Ochoa et al. (2021); (2) Ehret et al. (2012); (3*) Recalculated from Ehret et al. (2012) ($^{87}Sr/^{86}Sr$: using LOWESS 5 Fit 26/03/13 from McArthur et al., 2012, U–Pb: Using IsoplotR); (4) Muizon and Bellon (1986); (5) J.Barron (personal communication). YC: youngest cluster of grains; YG: youngest grain.

Label in Fig. 6	Locality	Sample ID	Lat.	Long.	Dating Method	Mean age (Ma)	Standard error (σ)	Confidence interval	Formation	Reference
1	**Quebrada Caracoles**	**MG-126**	−15.504	−74.725	U–Pb zircon (YC)	**1.45**	±0.04	0.077 (n = 7/7)	**Pongo**	This study
2	**Quebrada Caracoles**	**MG3-26**	−15.503	−74.746	U–Pb zircon (YC)	**1.95**	±0.03	0.065 (n = 5/6)	**Caracoles**	This study
3	Cerro Amarillo	MG3-57	−15.551	−74.722	U–Pb zircon	2.70	±0.04	0.68 (n = 3/4)		1
4	Cerro Amarillo	MG3-09	−15.551	−74.721	U–Pb zircon	5.65	±0.03	0.089 (n = 5/6)	**Pisco**	1
5	Quebrada Caracoles	MG-117 A	−15.502	−74.754	U–Pb zircon	4.54	±0.06	0.119 (n = 2/4)		1
6	Yauca Depressions	MG-138 A	−15.655	−74.587	U–Pb zircon	4.85	±0.04	0.086 (n = 14/17)		1
7	**Yauca Depressions**	**SAC 20–18-T1**	−15.654	−74.790	87Sr/86 Sr (in shark teeth)	**4.85**	±0.15	NA		This study
8	**Yauca Depressions**	**SAC 20–20-T1**	−15.656	−74.591	87Sr/86 Sr (in shark teeth)	**5.10**	±0.15	NA		This study
9	**Yauca Depressions**	**SAC 20–20-T2**	−15.656	−74.591	87Sr/86 Sr (in shark teeth)	**5.35**	±0.15	NA		This study
10	Sacaco – Chacra area	MG4-1Mz	−15.551	−74.736	U–Pb zircon	5.74	±0.06	0.706 (n = 2/3)		1
11	Sacaco – Chacra area	DV 514-2 Snee	Unknown	Unknown	Ar–Ar	5.75	±0.05	NA		2
12	Sacaco – Chacra area	–	Unknown	Unknown	87Sr/86 Sr (in CaCO3 shells)	5.76	6.2–5.45	NA		3*
13	Sacaco – Chacra area	MG3-25	−15.551	−74.737	U–Pb zircon	5.85	±0.03	0.060 (n = 35/36)		1
14	**Sacaco – Chacra area**	**MUSM 4664**	−15.548	−74.729	87Sr/86 Sr (in shark teeth)	**5.65**	±0.10	NA		This study
15	**Sacaco – Chacra area**	**MUSM 4665**	−15.521	−74.748	87Sr/86 Sr (in shark teeth)	**5.45**	±0.10	NA		This study
16	Sud-Sacaco	–	Unknown	Unknown	87Sr/86 Sr (in CaCO3 shells)	5.9	6.25–5.52	NA		3*
17	**Sud-Sacaco**	**MG4-25**	−15.585	−74.736	U–Pb zircon (YG)	**6.28**	±0.05	n = 1		This study
18	Sud-Sacaco	–	Unknown	Unknown	87Sr/86 Sr (in CaCO3 shells)	6.55	7.2–6.1	NA		3*
19	Sud-Sacaco	–	Unknown	Unknown	U–Pb zircon	7.2	±0.20	NA		3*
20	**Sud-Sacaco West**	**SAC 20–29-T1**	−15.584	−74.712	87Sr/86 Sr (in shark teeth)	**6.15**		NA		This study
21	**Sud-Sacaco West**	**SAC 20–29-T2**	−15.584	−74.712	87Sr/86 Sr (in shark teeth)	**5.85**		NA		This study
22	**Sud-Sacaco West**	**86DV432–1**	−15.34	−74.43	Diatom Biostratigraphy	**< 5.6**	NA	NA		Unpublished
	Sud-Sacaco West	**99DV1241–1**	−15.33	−74.45	Diatom Biostratigraphy	**< 5.6**	NA	NA		5
23	**Sud-Sacaco West**	**MG4-01**	−15.571	−74.728	U–Pb zircon (YG)	**6.62**	±0.10	n = 1		This study
24	**Montemar**	**MG4-06**	−15.582	−74.743	U–Pb zircon (YC)	**6.336**	±0.035	0.274 (n = 3/3)		This study
25	Montemar	–	Unknown	Unknown	87Sr/86 Sr (in CaCO3 shells)	7.15	8.25–6.52	NA		3*
26	Aguada de Lomas	Tuff 44	Unknown	Unknown	K–Ar biotite	7.93	±0.40	NA		4
27	Aguada de Lomas	Tuff 44	Unknown	Unknown	K–Ar biotite	8.04	±0.40	NA		4
28	Aguada de Lomas	Tuff 45	Unknown	Unknown	K–Ar biotite	8.85	±0.66	NA		4
29	**Yauca Road Cut**	**MG3-54**	−15.67	−74.532	U–Pb zircon (YG)	**7.40**	±0.30	n = 1		This study
30	**Yauca Road Cut**	**SAC 20–22-R2**	−15.67	−74.532	87Sr/86 Sr (in CaCO3 shells)	**7.25**	±0.25	NA		This study
31	**Aguada de Lomas (C. Vildoso)**	**MG6-09**	−15.513	−74.798	Diatom Biostratigraphy	**[6.2–5.6]**	NA	NA		This study
32	**Aguada de Lomas (Pascual)**	**MG-63**	−15.503	−74.827	U–Pb zircon (YC)	**9.21**	±0.08	0.485 (n = 3/4)		This study
33	El Jahuay (Alto Grande)	Tuff 1	Unknown	Unknown	K–Ar biotite	9.38	±0.47	NA		4
34	El Jahuay (Alto Grande)	Tuff 1	Unknown	Unknown	K–Ar biotite	9.63	±0.48	NA		4
35	El Jahuay (Alto Grande)	–	Unknown	Unknown	U–Pb zircon	9	±0.4	NA (n = 1/55)		3*
-	El Jahuay (Alto Grande)	–	Unknown	Unknown	87Sr/86 Sr (in CaCO3 shells)	7.35	8.55–6.50	NA		3*

occasionally contain shell debris of bivalves and gastropods. A 50-cm-thick ash layer (MG3-54; Fig. 3) was sampled for U–Pb radiometric dating, and one of the shell banks containing was also sampled for strontium isotopic analyses (SAC20-22-R5; Fig. 3). The top of the succession is irregularly cut by a Quaternary conglomerate.

Montemar: The Montemar locality extends for close to 10 km parallel to the coastline (Fig. 3). Continuous outcrops of significant thickness (greater than 10 m) are limited, however, and frequently covered by eolian deposits. Therefore, the characterization of the Montemar succession relies on the integration of available rock exposures. This locality includes the MTM fossiliferous level associated with the Pisco Formation, which was first described by Muizon and DeVries (1985). We have assessed the chronostratigraphic framework for this locality by integrating two stratigraphic sections (Sections S4 and S5 in Fig. 3). Rock exposures at the Montemar locality are composed of medium-grained gray sandstone-dominated intervals containing cm-thick yellow sandstones, hardgrounds, and shell beds. Sandstone beds vary from massive to parallel-laminated, sometimes include convolute structures, and exhibit a crude inverse gradation. Bioturbation becomes abundant at the top of each stratum. An erosive surface, identified as the Mio-Pliocene unconformity by Muizon and DeVries (1985), occurs towards the top of section S5. An ash level from section S5, below the unconformity, was sampled for U–Pb geochronology (MG4-06; Fig. 3).

Sud-Sacaco West: The rock record from the Sud-Sacaco West locality was studied by integrating two almost continuous stratigraphic sections (Sections S5 and S6 in Fig. 3) from the same areas visited by Muizon and DeVries (1985). As occurs at the Montemar locality, rock exposures at Sud-Sacaco West are uncommon, as the landscape is mostly flat, covered by eolian sands, or cut by younger gypsum or late Pleistocene shell terraces. Sedimentary rocks from the Sud-Sacaco West locality are associated with the Pisco Formation and show similar lithological characteristics to those from the Montemar locality, except that indurated fossiliferous sandstone beds appear to be more frequent. Sandstones, in general, are medium-to coarse-grained and are poorly sorted with variable fractions of silt and bioclasts. Two ashy sandstone beds (MG4-25 in Section S5 and MG4-01 in Section S6; Fig. 3) and two shark teeth (SAC 20–29 in Section S6; Fig. 3) were sampled for radiometric and strontium isotopic dating, respectively. Diatom biostratigraphic data from two samples collected in this locality (samples DV432-1 and DV1241-1 in Fig. 3), and independently analyzed in 1987 by H. Schrader (then with the College of Oceanography, Oregon State University, Oregon, USA) and in 2021 by J. Barron (United States Geological Survey, California, USA), are also reviewed and integrated into our chronostratigraphic framework. Sample DV432-1 was collected at the base of the Sud-Sacaco West locality.

Sacaco Chacra: The stratigraphic section from the Sacaco Chacra locality is shown in Section S7 (Fig. 3). The succession is located to the north of the Panamerican Highway, close to the Sacaco Paleontological Museum (see Fig. 3). The Sacaco Chacra locality is one of the best known fossiliferous localities associated with the Pisco Formation in the southern margin of the basin. The succession includes medium-grained yellow sandstones intercalating with shell banks dominated by *Anadara chilensis* and *Dosinia ponderosa* (see Appendix A). Further lithological features and U–Pb age constraints are described in Ochoa et al. (2021). For this study, two shark teeth were sampled for strontium chemostratigraphy (MUSM 4664 and MUSM 4665; Fig. 3).

Yauca Depressions: This locality is located between the valleys of the Acarí and Yauca rivers, a few hundred meters southwest of the Panamerican Highway (Fig. 3). Outcrops occur within small and isolated depressions, that are often covered by eolian sands or cut by multiple Pleistocene-age shell and gypsum terraces. Available rock exposures indicate that Mio-Pliocene sedimentary rocks from the Pisco Formation unconformably overlie igneous basement rocks (Section S8 in Fig. 3). The succession is formed by alternations of immature sandstones, calcareous mudstones, and several 10 to 20 cm-thick shell banks. The top of the succession is cut by the Panamerican Highway. A comprehensive lithological description can be found in Ochoa et al. (2021). Three shark teeth samples were collected and processed for strontium isotopic analysis (Fig. 3).

Cerro Amarillo: This locality is named after a hill (cerro in Spanish) that is located to the west of the Sacaco Chacra locality and about 1 km to the northeast of the Panamerican Highway (see Fig. 3). The stratigraphic section is 70 m thick, running parallel to a secondary road going to the Bella Union village. The lithostratigraphic features and malacological content of the section were addressed in great detail by DeVries (2020). The Cerro Amarillo locality encompasses sedimentary rocks from the Pisco and Caracoles formations. The Pisco Formation is formed by alternations of gray sandstones intercalating with 10–20 cm-thick yellowish sandstone and shell beds. An erosional angular unconformity separates the Pisco unit from the overlying Caracoles Formation (Fig. 3; DeVries, 2020; Ochoa et al., 2021). The latter formation consists of yellowish silty sandstones, fine to medium-grained sandstones, and cm-thick diatomaceous sands. Sandstones show an upward-coarsening trend. Shell lenses and banks also become thicker and frequent to the top of the succession (Fig. 3). Sediments from the Pongo Formation are found uphill at this locality, but are not included here as it was not possible to describe a continuous succession because of the frequent presence of younger gypsum terraces (Appendix A). At this locality, the uppermost rocks from the Pisco Formation are dated as 5.64 ± 0.03 Ma; whereas the lowermost beds from the overlying Caracoles Formation are dated as 2.7 ± 0.03 Ma (Ochoa et al., 2021).

Quebrada Caracoles: This locality corresponds to the type section of the Caracoles Formation (DeVries, 2020). It is located 5 km to the northwest of the Sacaco Chacra locality. The base of the section can be accessed following a local road towards a cement mine, continuing upwards through the path of an intermittent stream, known as Quebrada Caracoles (Fig. 3). The course of this stream offers continuous exposures of the Pisco, Caracoles, and Pongo formations. The Pisco Formation, cropping out only at the eastern margin of the locality, is composed of medium-grained immature sands intercalated with shell banks, indurated gray silt- and sandstone beds, and cm-thick diatomite and chert layers (Fig. 3). The age of these rocks has been determined to be 4.54 ± 0.06 Ma (Ochoa et al., 2021). As in the Cerro Amarillo locality, an erosional angular unconformity separates the Pisco and Caracoles formations. Above this erosional surface, the succession follows with ~30 m thick of medium to coarse bioclastic sandstones, alternating with shell banks dominated by venerids (*Dosinia*, *Amiantis*, *Cycinella*, and especially *Pitar*), cirripeds, and gastropods. The Caracoles-Pongo transition also corresponds to an erosional disconformity, which unlike the Pisco-Caracoles angular unconformity, is harder to identify in the field. Above the disconformity, the Pongo succession is composed of immature coarse sandstones intercalated with polymictic conglomerates and *Crepidula*-dominated shell banks and beds. Some of these *Crepidula* beds are prominent and continuous, thus can be used as regional marker beds (Fig. S2 in Appendix A). The top of the succession is cut by recent gypsum terraces. A thin ash level occurring close to the top of Section S10 (MG-126; Fig. 3) was sampled for U–Pb geochronology.

Quebrada Pongo: This locality contains the type section of the Pongo Formation (DeVries, 2020). The Pongo locality is situated 1 km to the west of the Quebrada Caracoles locality (Fig. 3). The section starts at the base of an intermittent stream (Quebrada Pongo), and continues uphill. To the west, the Pongo unit reaches the hills surrounding the Aguada de Lomas locality to the north (section S1b in Fig. 3). The succession at Quebrada Pongo is dominated by brown to greenish medium-to-coarse immature sandstones, intercalating with centimeter-thick silty sandstones, pebbly-cobbly conglomerates, and prominent shell beds (Fig. 3). Sandstone packages are either massive or have an incipient plano-parallel stratification. No ash layers were distinguished at this locality. Further details on the type section and the Pongo Formation can be found in DeVries (2020).

4.2. Chronostratigraphic results

A comprehensive summary of the U–Pb, strontium-based and biostratigraphic ages established herein, along with other dates existing for the Sacaco sub-basin, is presented in Table 1 and Fig. 6.

Age constraints for the Pisco Formation: Our results indicate that the base of the succession at the Aguada de Lomas locality is Tortonian, having an $^{238}U/^{206}Pb$ mean age of 9.205 ± 0.08 Ma (Fig. 4A). The sedimentary succession from the Yauca Road Cut section is also Tortonian, ranging between 7.4 and 7.2 Ma based on a single grain with a $^{238}U/^{206}Pb$ age of 7.4 ± 0.30 Ma (MG3-54; Fig. 4B) and a strontium-based age of 7.2 ± 0.15 Ma (Table 1). The upper part of the succession at the Montemar locality was deposited during the Messinian, with an $^{238}U/^{206}Pb$ maximum deposition age of 6.34 ± 0.03 Ma (MG4-06; Fig. 4C). The Sud-Sacaco West locality is late Messinian in age, with Sr isotopes ranging from 6.15 ± 0.15 to 5.85 ± 0.15 Ma and U–Pb maximum depositional ages of 6.28 ± 0.05 Ma (MG4-25; Figs. 4D) and 6.62 ± 0.10 Ma (MG4-01; Fig. 4D). Finally, Sr isotope results from shark teeth indicate a late Messinian age for the Sacaco Chacra (ranging between 5.65 ± 0.15 and 5.45 ± 0.15 Ma) and a latest Messinian-early Pliocene age for the Yauca Depressions (ranging between 5.35 ± 0.15 Ma and 4.85 ± 0.15; Table 1). Age constraints for the Caracoles and Pongo formations: Two ash samples from the Quebrada Caracoles locality provide maximum depositional ages for these sedimentary units. The lower sample, taken from the Caracoles Formation, yielded five zircons with a weighted mean age of 1.95 ± 0.03 Ma (MG3-26; Fig. 4E). The upper sample, collected from the Pongo Formation, yielded 15 zircon crystals with a weighted mean age of 1.45 ± 0.04 Ma (MG-126; Fig. 4F).

4.3. Zircon-population age patterns

Detrital zircons from the Sacaco sub-basin exhibit four distinctive age populations in the Pisco, Caracoles, and Pongo formations: a predominant Mio-Pleistocene signal (23–~1.2 Ma, n = 290) accompanied by a late Cretaceous (100-65 Ma, n = 76) and early Cretaceous (160-125 Ma, n = 108) component, with a Neoproterozoic component (850-735 Ma, n = 88) present only in the oldest samples (>6 Ma; Fig. 5). The presence and abundance of these four main signatures vary up-section. Additionally, few zircon crystals of Mesoproterozoic (n = 6), Paleoproterozoic (n = 3), and Mesoarchean (n = 2) ages are also present (Fig. 5).

5. Discussion

5.1. Age refinement of the sedimentary successions from the Sacaco sub-basin

In the Sacaco sub-basin, ages for the Pisco Formation had been assessed by dating rocks associated mainly with five fossiliferous levels, known as El Jahuay (Alto Grande; ELJ), Aguada de Lomas (AGL), Montemar (MTM), Sud-Sacaco West (SAS-W), and Sacaco (SAO; Muizon and DeVries, 1985; Muizon and Bellon, 1986; Ehret et al., 2012).

The first absolute ages for the Pisco Formation in the Sacaco sub-

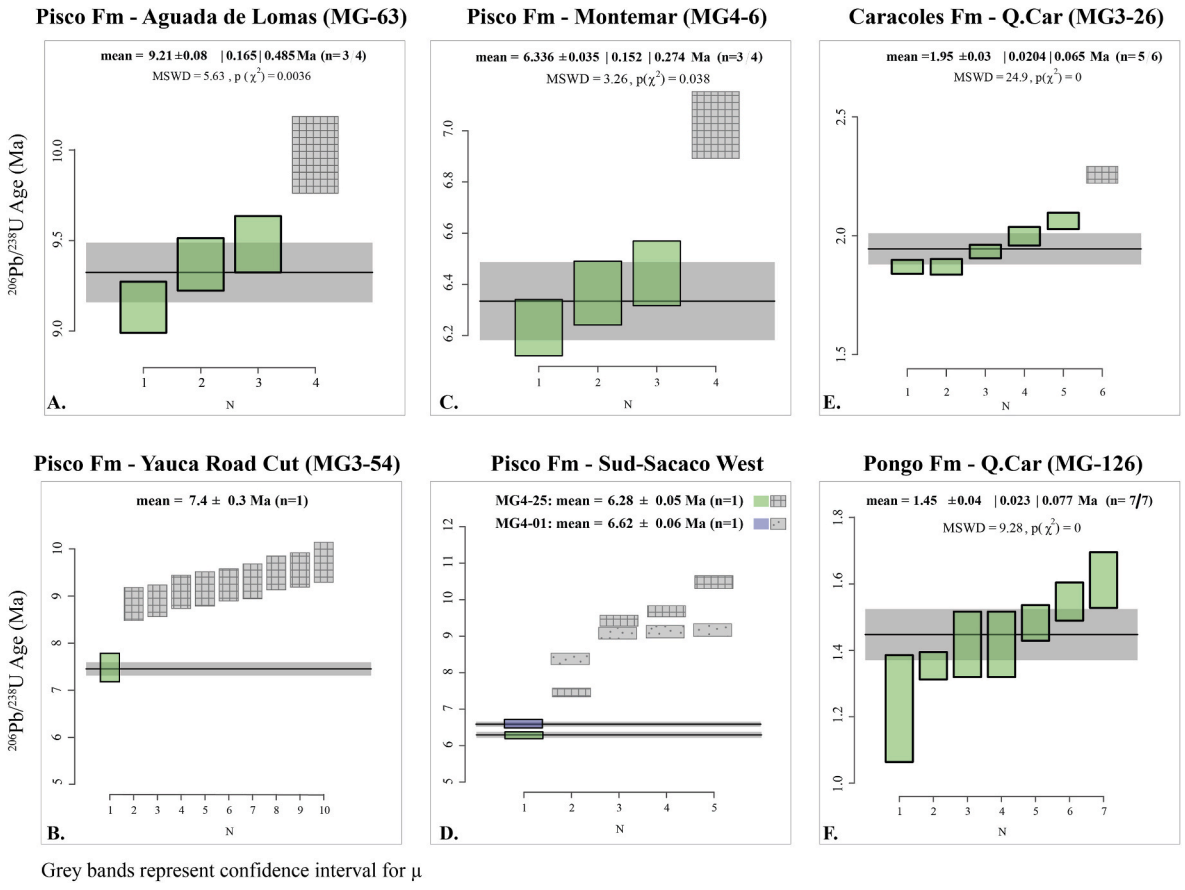

Fig. 4. U–Pb weighted mean ages (μ) for collected samples from the Sacaco sub-basin calculated from the youngest cluster of zircon crystals (YC) or youngest grain (YG). Green squares: zircon grains used for calculating weighted mean age. Crosshatched (dotted) squares: zircon grains outside 2σ of weighted mean age. Legend: mean = μ ± x |y | (z); where: μ: the weighted mean age, x: the standard error (σ) of μ, y: the width of the 100 (1-α) % confidence interval for μ (shown as a gray band on the plot). z: the approximate 100 (1- α) % confidence interval for t with overdispersion, calculated as $z = y\sqrt{MSWD}$. Further legend details can be found in Ludwig (2003) and Vermeesch (2018). Q. Car = Quebrada Caracoles.

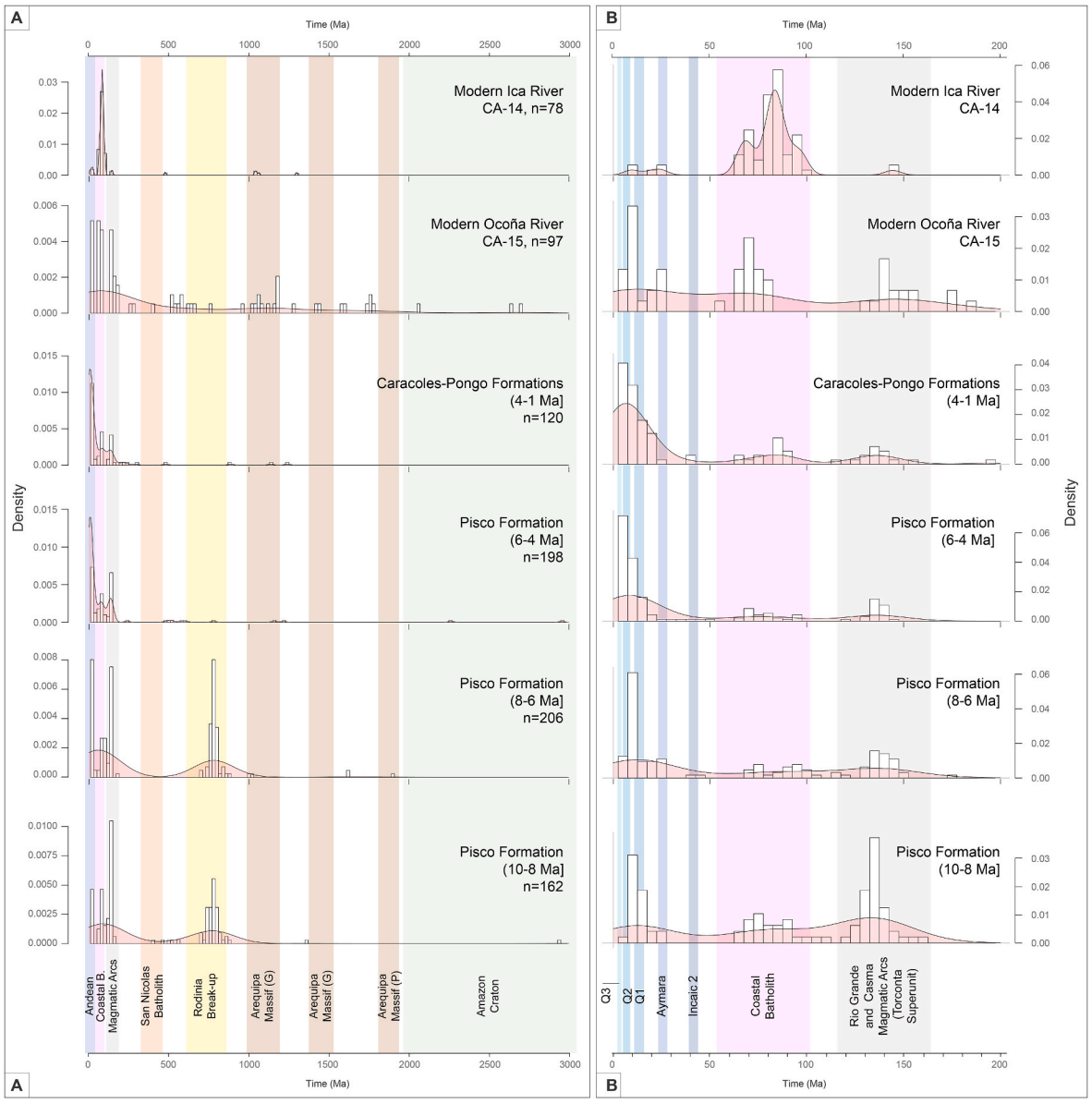

Fig. 5. Kernel density estimation (pink) and histogram plots (rectangles) for U–Pb weighted mean ages for the Sacaco sub-basin. **A)** Age distribution from 0 to 3000 Ma. **B)** Age distribution from 0 to 200 Ma. Samples were distributed in four time bins based on their maximum depositional ages, as follows: 10-8 Ma (MG-63; MG3-54; ELJ 2012), 8-6 Ma (MG4-01; MG4-21; MG4-25; SAS 2012), 6-4 Ma (MG-117 A; MG-138 A; MG3-25; MG3-09; MG4-1Mz), and 4-1 Ma (MG-126; MG3-26; MG3-57). For comparison, zircon distributions of two modern rivers from the area (CA14 and C15; Pepper et al., 2016) are shown in the two topmost panels. Statistical treatment and graphic presentation after Vermeesch (2018).

basin were provided by Muizon and Bellon (1980, 1986) through K–Ar radiometric dating on biotites. Relative ages were indicated based on the morphological evolution of various invertebrate and vertebrate groups (e.g., Muizon and DeVries, 1985; Muizon et al., 2004; DeVries, 2020). An age-revision of the sub-basin rocks was undertaken by Ehret et al. (2012) by integrating morphological traits of *Carcharodon* teeth, U–Pb geochronology, and strontium-based chemostratigraphy based on the LOWESS V.4 Fit table (McArthur et al., 2001). Additional radiometric dates for the Pisco Formation have been reported in different publications (see Ehret et al., 2012; DeVries et al., 2021), but have not yet been formally described yet. By contrast, the ages of the Caracoles and Pongo Formations had only been assessed through molluscan biostratigraphic data and considering the elevation of the Pleistocene terraces (DeVries, 2020). To better constrain the stratigraphy at the Sacaco sub-basin we integrated different dating techniques, as shown in Table 1. In the following paragraphs, we review existing and new age constraints, aiming to provide a robust chronostratigraphic framework for the Sacaco area.

5.1.1. *Pisco Formation*

The oldest known Pisco rocks from the Sacaco sub-basin occur at El Jahuay (Alto Grande) and include the ELJ vertebrate fossiliferous horizon. The locality was radiometrically dated as ~9.6–9.4 Ma by Muizon and Bellon (1986). Ehret et al. (2012) analyzed U–Pb zircon ages from the same tuff bed and found that the youngest grain yielded an age of 10 ± 1.0 Ma. We recalculated all U–Pb crystal ages from the same sample, and were able to constrained the age of the youngest crystal to 9.0 ± 0.40 Ma (sample El Jahuay-Alto Grande; Appendix B), supporting a Tortonian maximum depositional age for the succession as indicated by Muizon and Bellon (1986). Ehret et al. (2012) further reported a younger strontium-based age with a broad confidence interval (7.46 Ma; CI: 9.03–6.51 Ma). Given the radiometric ages (Ar–Ar and U–Pb), the El

Jahuay (Alto Grande) locality is considered as Tortonian in age, varying from ~9.6 to 9.0 Ma, and so it represents the oldest known succession with associated paleontological content from the Sacaco sub-basin (Fig. 6). As these successions lie directly on basement rocks (see Fig. 7A), the possibilities of having much older sedimentary rocks in the Sacaco area are remote.

The Aguada de Lomas locality contains more than 200 m of sedimentary rocks associated to the Pisco Formation (Brand et al., 2011), and it includes at least five different fossiliferous horizons (i.e., from oldest to youngest, Pascual, Sirenios, Hueso Blanco, the Water Wells, and Cerro Vildoso; see Fig. S1 in Appendix A). Our Section 1 contains the well-known AGL vertebrate-level of Muizon and DeVries (1985; Fig. 3). The MG-63 sample collected close to the base of the succession within the Pascual Zone (Fig. 3), yielded a U–Pb weighted mean age of 9.2 ± 0.08 Ma (Fig. 4A; Table 1). This radiometric date provides an approximate age for the lowermost sedimentary successions of the Aguada de Lomas locality (Pascual Zone) and expands its lower limit into the Tortonian. Three additional radiometric K–Ar ages from two tuffs (samples 44 and 45 in Muizon and Bellon, 1986) indicate an age between ~8.8 and 7.9 Ma for rocks associated to the AGL vertebrate-level (Table 1). Unfortunately, the geographic location and the stratigraphic position of these tuffs are indeterminate, hence a well-defined

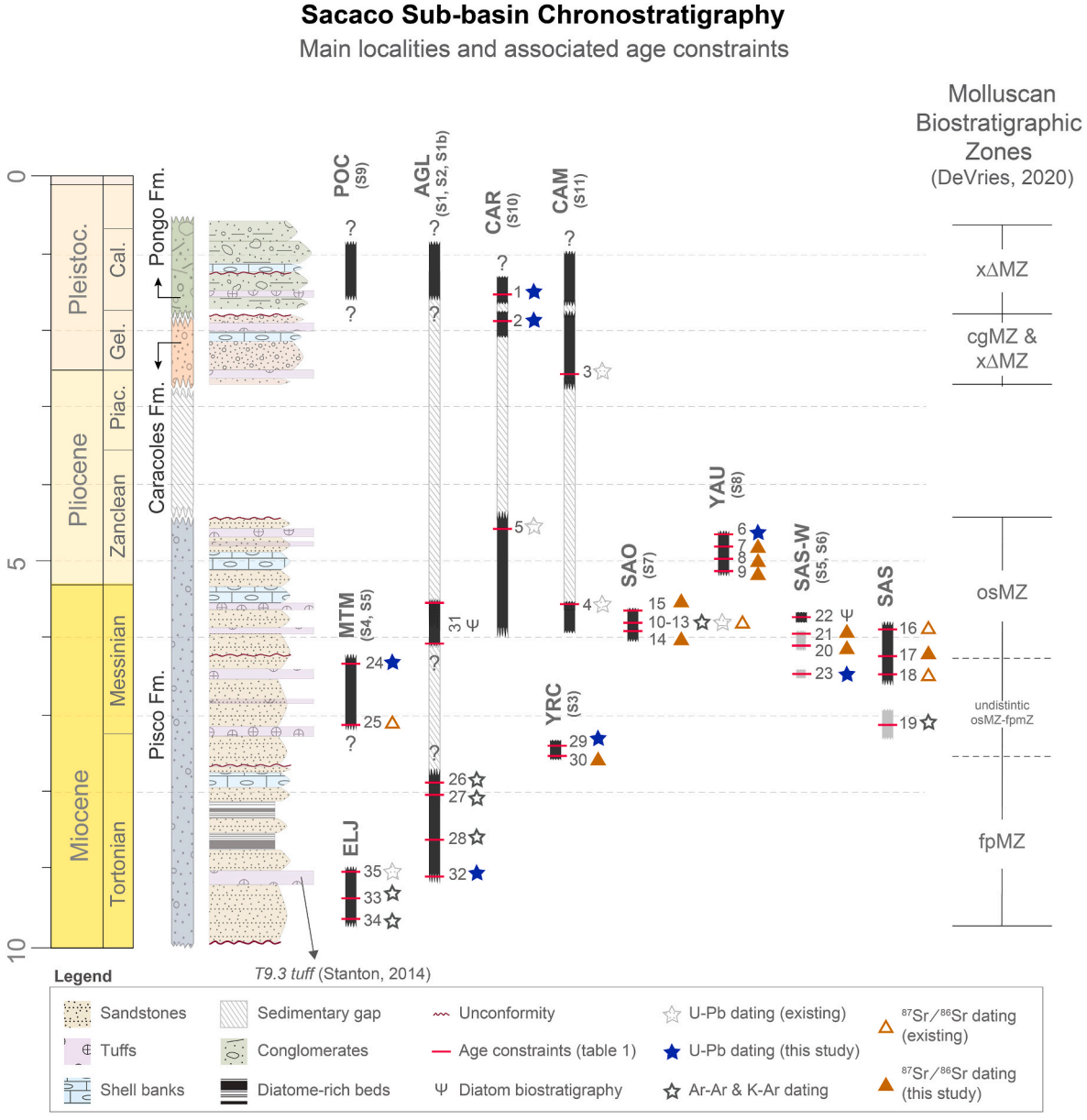

Fig. 6. Chronostratigraphic framework for late Miocene-Pleistocene deposits of the Sacaco sub-basin. Black bars represent the estimated time span of each studied locality. Roman numerals are associated to metadata presented in Table 1 (location, method, age confidence level, reference). Time constraints are as follows: filled stars correspond to U–Pb weighted mean ages (Ehret et al., 2012; Ochoa et al., 2021), empty stars to Ar–Ar radiometric dates (Muizon and Bellon, 1986), and triangles to $^{87}Sr/^{86}Sr$ based ages (Ehret et al., 2012). Molluscan biostratigraphic zones identified in the Sacaco sub-basin, according to DeVries (2020), are shown to the right. *Chorus frassinettii-Herminespina philippii* Molluscan Concurrent Range Zone (fpMZ); *Xanthochorus ochuroma-Herminespina saskiae* Molluscan Concurrent Range Zone (osMZ); Toothed Concholepas-*Chorus grandis* Molluscan Concurrent Range Zone (cgMZ); *Xanthochorus xuster*/transitional *Chorus grandis* Molluscan Concurrent Range Zone (xΔMZ); and *Acanthina unicornis-Xanthochorus cassidiformis* Molluscan Concurrent Range Zone (ucMZ). Localities names are as follow: El Jahuay (Altogrande; ELJ), Aguada de Lomas (AGL), Yauca Road Cut (YRC), Montemar (MTM), Sud-Sacaco (SAS), Sud-Sacaco West (SAS-W), Sacaco Chacra (SAO), Yauca Depressions (YAU), Cerro Amarillo (CAM), Quebrada Caracoles (CAR), and Quebrada Pongo (POC) Numbers in parenthesis accompanying localities' names correspond with sections shown in Fig. 3.

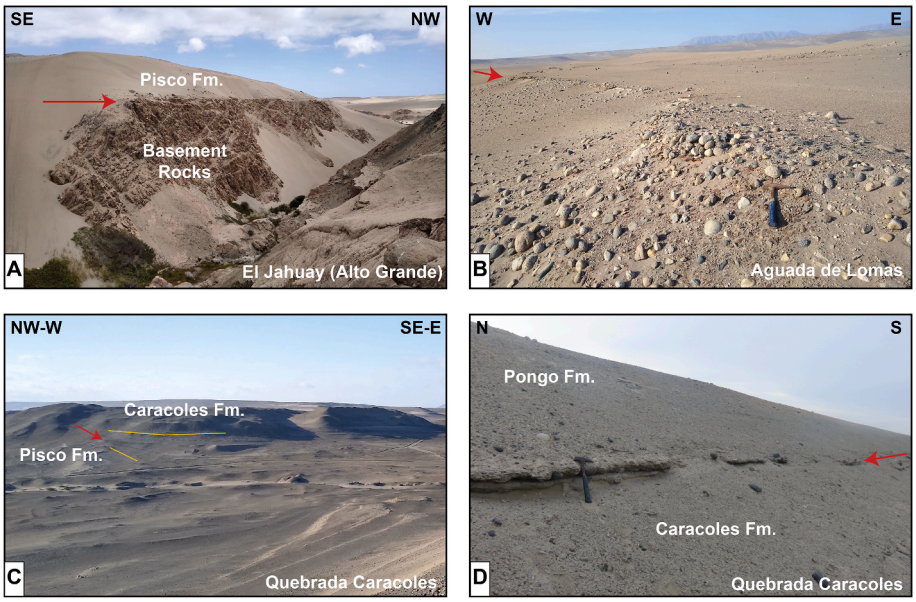

Fig. 7. Unconformities at the Sacaco sub-basin. **A)** Angular unconformity separating Basement rocks and the Pisco Formation at El Jahuay (Alto Grande). **B)** Intraformational unconformity at the Aguada de Lomas locality. **C)** Angular unconformity between the Pisco and Caracoles formations, as seen at mouth of the Quebrada Caracoles. **D)** Clastic sandstones of the Pongo Formation unconformably overlying bioclastic sandstones of the Caracoles Formation (Quebrada Caracoles).

chronology for the fossiliferous levels across the locality remains uncertain. Nonetheless, according to Lambert and Muizon (2013), both tuffs were collected close to the guide beds LM6 and LM7 of Brand et al. (2011; see Fig. 3), and so they provide an age to the Sirenios Zone (~25–27 m from the base of the Section S1; Fig. 3).

Towards the base of the Aguada de Lomas succession (~23 m from the base of the Section S1; Fig. 3), an intraformational unconformity occurs. In the field, it can be recognized based on the presence of two prominent conglomeratic beds, containing abundant igneous and metamorphic cobbles and boulders aligned to the bed's strike (Fig. 7B). A 10–15° difference is visible between the sediments at the bottom (So = 325/4, n = 3) and the overlying sandstone beds (So = 334/15, n = 5), reflecting the low-angle angular nature of this tectonic-driven unconformity. A coeval phase of surficial uplift has also been documented based on the incision history of the nearby Cotahuasi-Ocoña Canyon (~16°S; Schildgen et al., 2007). Both the age and the time gap encompassed by this unconformity are uncertain. However, its maximum age is constrained by the MG-63 sample collected to the base of the Aguada de Lomas succession (~9 m from the base of the Section S1; Fig. 3), which indicates that the unconformity is younger than 9.2 ± 0.08 Ma (Table 1). The minimum possible age is tentatively indicated as 8.85 Ma based on the Ar–Ar radiometric ages provided by Muizon and Bellon (1986), which according to Lambert and Muizon (2013) were collected close to the beds LM6 and LM7 of Brand et al. (2013), and so above the unconformity (~25–27 m from the base of the Section S1; Fig. 3).

The uppermost Pisco successions from the Aguada de Lomas occur at Cerro Vildoso and are unconformably resting over those from the Water Wells Zone (Fig. 3). An approximate age for the Cerro Vildoso beds was constrained based on the diatom content observed in two samples (Fig. 3). The diatom assemblage shows a distinctive Messinian provincial flora and includes the presence of *Thalassiosira hyalinopsis*, which has a First Appearance Datum (FAD) estimated to be 6.3 Ma (Barron, 2003; Appendix D). No occurrence of *Thalassiosira oestrupii* was reported (FAD 5.6 Ma; Barron, 2003), suggesting an age older than 5.6 Ma (J. Barron, pers. communication). Consequently, the sedimentary succession from the Cerro Vildoso is interpreted as being deposited between ~6.3 and 5.6 Ma. Based on the data presented, the Pisco succession cropping out at the Aguada de Lomas locality ranges from the Tortonian to the Messinian (9.2–~5.6 Ma) and would include a sedimentary hiatus at the base of Cerro Vildoso, which would have a maximum time-span from ~?7.9 to ~6.3 Ma. Nonetheless, the age of the lower boundary remains to be further defined, and so, too, its regional significance.

Next in the composite succession is the sedimentary succession from the Yauca Road Cut locality, which is found to range between 7-4-7.2 Ma (Fig. 4B; Table 1). This age is consistent with the presence of intermediate morphologies between *Xanthochorus stephanicus* and *X. ochuroma*, estimated to be younger than ~9 Ma but older than ~4.5 Ma (DeVries, 2020). Coeval to the Yauca Road Cut locality are the lowermost sedimentary strata from the Montemar locality. The Montemar locality was first defined as late Miocene based on the fossiliferous content of the homonymous vertebrate-bearing level (Muizon and DeVries, 1985). Almost three decades later, Ehret et al. (2012) provided a strontium-based absolute age of ~7.3 Ma (CI: 8.7–6.45 Ma; LOWESS V.4). We recalculated the age for the strontium ratios provided by them, by using the LOWESS V.5 table of McArthur et al. (2012), as ~7.15 Ma (CI: 8.25–6.52 Ma; Table 1). We further sampled a tuff bed (MG4-06) that occurs towards the upper part of the succession but below the erosive surface (Section S5; Fig. 3), and which yielded a U–Pb weighted mean age of 6.33 ± 0.03 Ma. Given the stratigraphic position of this sample, this radiometric age can be used as an approximation of the age of the Montemar's youngest rocks. Therefore, the Montemar locality would be late Tortonian-Messinian in age, spanning from ~7.15 to 6.3 Ma (Fig. 6). Nonetheless, the age of the oldest sedimentary rocks remains poorly constrained, due to the broad confidence interval and the unknown stratigraphic position of the previous strontium-based datum.

The Montemar locality is unconformably overlaid by the rocks from the Sud-Sacaco West locality (Section S5 in Fig. 3). Muizon and DeVries (1985) suggested a Pliocene age for the Sud-Sacaco West locality based on the co-occurrence of *Carcharodon carcharias*, *Ninoziphius* and *Delphinus*-like remains. Ehret et al. (2012) provided two late Miocene strontium-based ages, 6.59 Ma (CI: 10.77–2.5 Ma) and 5.93 Ma (CI: 6.35–5.47 Ma), which we updated to 6.55 Ma (CI: 7.2–6.1 Ma) and 5.9 Ma (CI: 6.25–5.52 Ma), respectively. Our strontium-based analyses from fossil shark teeth also indicate ages ranging from 6.2 to 5.8 Ma (Table 1). However, the diatom flora from two samples (86DV432-1 and 99DV1241-1; Appendix D), includes the warm-water *Thalassiosira oestrupii* (see Appendix D), with a FAD in the Pacific Ocean of 5.6 Ma (Barron, 2003). Considering that one of these samples (86DV432-1) was

collected at the base of the Sud-Sacaco West succession, the age of the locality is regarded as late Messinian, likely being younger than 5.6 Ma (Fig. 6). As for the U–Pb geochronology, the MG4-25 sample, collected from Section S5 (Fig. 3), yielded only one zircon crystal with an estimated radiometric age of 6.28 ± 0.05 Ma (green square in Fig. 4D), and the overlying MG4-01 sample yielded one zircon crystal with an older age of 6.6 ± 0.10 Ma (blue square in Fig. 4D; see Section S6, Fig. 3), indicating a maximum depositional age of 6.28 Ma for the Sud-Sacaco West locality. Based on the diatom flora, we estimate an age younger than 5.6 Ma for the Sud-Sacaco West locality. A late Messinian age is also supported by the faunal resemblance between this and the Sacaco Chacra locality (Muizon and DeVries, 1985; Brand et al., 2011).

The intraformational unconformity occurring between the uppermost rocks from Montemar and those from Sud-Sacaco West was first identified by Muizon and DeVries (1985), based on its lithological characteristics and the distinctive fossiliferous content existing below and above it (Section S5 in Fig. 3). According to them, convoluted and cross-bedded gray sandstone beds containing transitional forms of the Miocene *Isurus hastalis* overlie pale gray siltstone beds with presence of the serrated *Carcharodon carcharias*, which led them to indicate a late Miocene-early Pliocene age for the unconformity. In light of the new age controls existing for the Montemar and Sud-Sacaco West localities, the erosive event that gave rise to this surface occurred during the late Miocene (Messinian). The lower age limit of the hiatus is restricted to 6.3 Ma, based on the youngest U–Pb weighted mean age found at Montemar (6.3 Ma; MG4-06 in Table 1). The upper age limit, although poorly defined, is still placed within the late Miocene, as the overlying rocks from the Sud-Sacaco West locality yielded a diatom-based biostratigraphic age younger than 5.6 Ma (Appendix D). From this data, the unconformity can be referred to as a Messinian unconformity possibly occurring around 6.3 Ma up to at least 5.6 Ma. It is of interest to note that sediment accumulation at the Aguada de Lomas locality (Cerro Vildoso) appears to have been restored around ~6.3 Ma after an arguably prolonged sedimentary gap (?7.9 to 6.3 Ma). Muizon and DeVries (1985) associated the origin of this unconformity with subaerial erosive processes after a sea-level drop. We found no indication of a tectonic-related origin during our field observations. However, the detrital zircon populations recovered from the sub-basin indicate that there is a change in provenance source at 6 My (Fig. 5), which could either be the result of some tectonic event around 6.3-?6.0 Ma or the exhaustion of the sediment source (see section 5.4).

The Sacaco Chacra locality includes all Pisco rocks occurring around the Paleontological Museum of Sacaco, as well as the traditional fossiliferous SAO horizon. Until recently the Sacaco Chacra locality represented the youngest vertebrate-bearing succession of the sub-basin (Ochoa et al., 2021). It was originally dated as Pliocene (3.9 Ma) based on K–Ar radiometric dating (Muizon and Bellon, 1980). Ehret et al. (2012) provided an older age of 5.89 Ma (CI: 6.76–4.86 Ma) based on strontium chemostratigraphy, which we recalculated as 5.76 Ma (CI: 6.2–5.45 Ma). We found similar strontium-based isotopic ages from two shark teeth that yielded ages between 6.15 and 5.85 ± 0.15 Ma (Table 1). Messinian dates, ranging between 5.8 and 5.75 Ma, were also found through Ar–Ar and zircon U–Pb radiometric methods by different authors (Table 1; Ehret et al., 2012; Ochoa et al., 2021; DeVries et al., 2021 [see 87-DV514 2Snee]). These combined results support a Messinian age for the Sacaco Chacra locality (Fig. 6). Furthermore, rocks from the Sacaco Chacra locality can be followed upwards into the Cerro Amarillo locality, where zircon U–Pb ages provided a maximum depositional age of ~5.6 Ma for the uppermost successions from the Pisco Formation (Ochoa et al., 2021). Consequently, the sedimentary rocks from the Sacaco Chacra locality can be considered as Messinian ranging from 5.9 to ~5.7 Ma (Fig. 6).

The youngest known rocks from the Pisco Formation in the Sacaco sub-basin crop out in the Yauca Depressions and Quebrada Caracoles localities (Ochoa et al., 2021). Both have yielded abundant vertebrate remains over the last 20 years (e.g., Muizon et al., 2004; Varas-Malca et al., 2019; Ochoa et al., 2021). Strontium isotopic data and U–Pb geochronology indicate a maximum depositional age of 4.8 Ma for the Yauca Depressions locality and of ~4.5 Ma for the Quebrada Caracoles locality (Table 1).

5.1.2. Caracoles Formation

The Pisco Formation is overlaid by the Caracoles Formation in the Sacaco sub-basin (see sections 10 and 11 in Fig. 3). The age of the Caracoles Formation ranges from the Piacenzian to the Gelasian (~2.7 up to at least 1.9 Ma, samples MG3-26 and MG3-57 in Table 1). These results are consistent with previous age assignments based on biostratigraphic data (DeVries, 2020). The contact between the Pisco and the overlying Caracoles formations corresponds to a low-angle angular unconformity (5-10°), that has been identified at the Cerro Amarillo and Quebrada Caracoles localities (Fig. 7C). A full description of the unconformity's lithological expression and extension across the sub-basin can be found in DeVries (2020), who referred to it as the "*Dientes Unconformity*" because of the large number of abraded shark teeth it contains. Based on the malacological content and radiometric dating, an early Pliocene age was recently ascribed to it (DeVries, 2020; Ochoa et al., 2021). The age of the lower boundary was determined at 5.6 Ma in Cerro Amarillo and at 4.5 Ma in Quebrada Caracoles, while the upper limit was dated at 2.7 Ma (Cerro Amarillo; Table 1). The unconformity thus represents a time gap of 1.8 My and its origin is related to an early Pliocene phase of regional surface uplift (Ochoa et al., 2021).

5.1.3. Pongo Formation

The Caracoles Formation is unconformably overlain by the Pongo Formation (Fig. 7D), the youngest marine unit from the Sacaco sub-basin. An approximate upper age of 1.45 Ma for the Pongo Formation is indicated by sample MG-126 (Fig. 4F) and so an approximated age spanning from the late Gelasian to the early Calabrian (early Pleistocene) is estimated, considering the youngest known age of the underlying Caracoles unit (MG3-26 in Fig. 4E). A previous late Pliocene-early Pleistocene age assignment based on molluscan biostratigraphic data supports this result (DeVries, 2020). Though the ages estimated for the Pongo Formation are a reasonable approximation of its absolute age, they should be considered cautiously because the unit changes in thickness towards the north (east of Aguada de Lomas; Fig. 1B), and so younger sedimentary rocks can exist in this direction. Additionally, the age of the lower boundary may be younger than suggested, since it has been estimated from an ash-level occurring below the Caracoles-Pongo disconformable boundary and the time gap represented by this sedimentary hiatus remains unknown to date.

An additional intraformational unconformity exists within the Pongo Formation ("*Intra-Pongo*" unconformity of DeVries, 2020), separating the unit into the Pongo-1 and Pongo-2 sequences. We identified this erosive surface in exposures along the Quebrada Pongo and Quebrada Caracoles. This *Intra-Pongo* unconformity as well as the Caracoles-Pongo unconformity are thought to have formed during the late Pliocene or Pleistocene, in response to eustatic sea-level fluctuations (DeVries, 2020). During our field observations, we found no indication of a tectonic-related origin for any of these erosive surfaces. Therefore, we also consider these sedimentary breaks as resulting from third-order eustatic sea-level changes. As mentioned before, there are still no absolute time constraints for these unconformities to date. Therefore, we have to rely on two radiometric dates enclosing these erosive surfaces. The oldest existing age indicates a maximum depositional age of 1.95 Ma for the Caracoles Formation, while the youngest date provides a maximum age of 1.45 Ma for the upper allosequence (Pongo-2) of the Pongo Formation (MG3-26 and MG-126, respectively; Table 1; Fig. 3). According to these radiometric ages, both surfaces were developed after sea-levels changes occurring during the early Pleistocene, between 1.9 and 1.4 Ma. These ages would favor the scenario 2 of DeVries (2020), in which sea level drops of up to 70–80 m occurring between the Marine Isotopic Stages MIS 50 and 44 would have given rise to both the

Caracoles-Pongo and the *Intra-Pongo* unconformities.

5.2. Integration with the existing molluscan biostratigraphic zonation

Muizon and DeVries (1985) were pioneers in the study of the stratigraphic distribution and evolution of vertebrate and invertebrate faunas from the EPB. They proposed a late Miocene-Pleistocene biostratigraphic zonation specifically tailored to the Sacaco sub-basin based on the occurrence of several molluscan taxa. This zonation contains five recognizable biozones (*Ficus* zone, *Acanthinonucella* zone, *Anadara* zone, *Crepidula uncinatus* zone, and *Crepidula [Crepipatella] dilatata* zone) and was recently reassessed by DeVries (2020), who defined six concurrent molluscan zones after the revision and inclusion of new muricoid taxa.

The biochronology of the updated molluscan zonation of DeVries (2020) relies on the stratigraphic position and existing chronostratigraphic information from several localities within the Sacaco sub-basin and one extrabasinal section located 50 km to the south of the Sacaco sub-basin (Huacllaco Section [Fig. 1A; 15.74°S, 74.17°W]; see DeVries, 2020 for further details). Here, we will briefly review and update the time span of these molluscan biozones based on the new time constraints (Fig. 6). The oldest biostratigraphic zone corresponds to the *Chorus frassinettii-Herminespina philippii* molluscan concurrent range Zone (fpMZ; ~10 to 6 Ma). This zone is fully identified at the El Jahuay (Alto Grande) and Aguada de Lomas localities (Fig. 6). The second oldest zone is the *Xanthochorus ochuroma-Herminespina saskiae* molluscan Concurrent Range Zone (osMZ; ~6 to 4 Ma). The osMZ is present at the Sud-Sacaco West, Sacaco, and Yauca Depressions localities, as well as within the Pisco rocks from the Quebrada Caracoles and Cerro Amarillo localities. Neither the fpMZ nor the osMZ were recognized at the Yauca Road Cut and Montemar localities, the only areas containing deposits accumulated between 7.4 and 6.3 Ma. Consequently, these rocks are tentatively placed within an fpMZ-osMZ indistinct zone (Fig. 6). The top of the osMZ was defined by DeVries (2020) as 4 Ma based on a radiometric date provided by Muizon and Bellon (1980) for sedimentary successions cropping out at the Sacaco Chacra locality (associated with the SAO level of Muizon and DeVries, 1985), which were traditionally considered as the youngest preserved Pisco deposits at the Sacaco sub-basin. A recent assessment of the last known Pisco rocks from the sub-basin shows that they accumulated only until 4.5 Ma (Ochoa et al., 2021). Consequently, the osMZ age should be defined as ranging from ~6 to 4.5 Ma.

The next youngest zones, the *Acanthina triangularis-Herminespina mirabilis* Molluscan Concurrent Range Zone (tmMZ; 4-3 Ma) and the toothed *Concholepas-Chorus grandis* Molluscan Concurrent Range Zone (cgMZ; 3-2 Ma), are either not present or cannot be recognized at the Sacaco sub-basin (DeVries, 2020). Nonetheless, as the tmMZ's lower limit was originally defined based on the age of the last preserved Pisco sedimentary successions, it should equally be constrained as ranging from 4.5 to 3 Ma. The last biozone recognized within the sediments here studied corresponds to the *Xanthochorus xuster/transitional Chorus grandis* Molluscan Concurrent Range Zone (xΔMZ; ~2-1 Ma). This biozone is recognized within sediments of the Pongo Formation (Fig. 6), which are radiometrically dated as accumulated from ~1.9 to at least 1.4 Ma. These absolute dates are comparable to the original biochronology defined for the xΔMZ (DeVries, 2020).

5.3. Correlation with the northern EPB sedimentary allosequences

The stratigraphic architecture of the Pisco Formation in the northern EPB mostly relies on work carried out in the Ica River Valley from Ocucaje to Zamaca (14.3–14.7°S; Brand et al., 2011; Esperante et al., 2015; Di Celma et al., 2017, 2018a, 2018b; Bosio et al., 2020). Recently, three fining-upward transgressive sequences (see Fig. 2; P0, P1, and P2; Di Celma et al., 2017, 2018) separated by three unconformities that converge and merge landward into a single surface, were defined for the Miocene sedimentary rocks from the Ica River Valley. According to Di Celma et al. (2018), the origin of all allomember-bounding surfaces is related to eustatic changes and shows no evidence of subaerial exposure, suggesting only changes in water-depth and sedimentary facies. However, some indicators of subaerial erosion locally can occur between unconformities (e.g., P0–P1 boundary at Yesera de Amara; DeVries and Jud, 2018). Although these three allosequences and associated erosional unconformities have been fully identified at numerous rock exposures around the Ica River Valley (e.g., Di Celma et al., 2018; DeVries and Jud, 2018; Bosio et al., 2019), no correlation has yet been established with sedimentary successions cropping out outside the Ica River Valley (e.g., Puente Huamaní) or the Sacaco sub-basin.

The P0 is the lowermost allosequence and was deposited during the Langhian-Serravallian (Fig. 2; 14.8–12.4 Ma; Bosio et al., 2020; DeVries et al., 2021). To date, in the Sacaco sub-basin there are no chronostratigraphically correlatable sequences to those of P0, as the oldest known Pisco deposits in the sub-basin are of Tortonian age (9.6–9.0 Ma; Fig. 6). The P0 allosequence is bounded at the top by the PE0.1 erosional surface, which places it into contact with the overlying P1 allomember. The P1 was deposited during the Tortonian (from ~9.5 to 8.6 Ma; Di Celma et al., 2017; Bosio et al., 2019) according to existing ages from the western Ica River Valley. However, new radiometric dates and stratigraphic correlations from the Laberinto area (Sula Section in the eastern flank of the Ica River Valley, see Fig. 1A) suggest that the P1 allomember would also include rocks as old as 12.5 Ma (DeVries and Jud, 2018; DeVries et al., 2021). Furthermore, a new formation (provisionally named Mature Formation, ~10-9 Ma) correlative with the P1 allomember was defined by DeVries et al. (2021) for sedimentary rocks occurring on the eastern flank of the lower Ica River Valley (Mature Pampa) in the northern EPB (see Fig. 2). Coeval rocks to those of the P1 sequence and the Mature Formation in the Sacaco sub-basin are found at the El Jahuay (Alto Grande), Yauca Road Cut, and (lower) Aguada de Lomas localities (Fig. 6). The P1 allosequence is bounded at the top by the PE0.2 erosive surface, which encompasses about 200 ky (Bosio et al., 2019). A correlatable surface to the PE0.2 has yet to be identified in the Sacaco sub-basin. However, the unconformity occurring at the base of the Aguada de Lomas succession, whose age has been broadly constrained as younger than 9.21 Ma but older than 8.85 Ma, is a suitable candidate to correlate with the PE0.2 surface. This correlation is proposed considering that in the northern Ica River Valley (at Cerros Mamá e Hija) the PE0.2 occurs few meters above two closely spaced ash beds, which have been dated as 9.22 ± 0.04 Ma and 9.14 ± 0.04 Ma (DV 484 3Asnee and DV 484-3Bsnee; see DeVries and Jud, 2018). One of these beds might thus correspond to the ash bed sampled at the base of Aguada de Lomas (sample MG-63 in Fig. 3). However, it also needs to be considered that, at least at the Sacaco area, there may not be a simple P0/P1/P2 allostratigraphic pattern because of diachronous transgressive events, substantial pre-Pisco topography (given the basement rocks existing around the Montemar and Sud Sacaco-east localities), and syndepositional tectonic activity.

The aforementioned 9.2 Ma ash beds appear to represent a synchronous and effectively correlatable event, taking place before the P1–P2 transition. In the northern EPB, at least nine ash horizons of similar age (9.2 ± 0.03 Ma) have been identified to occur associated to comparable stratigraphical sequences (Zancones [Z1, Z2, Z3; Stanton, 2014), Cerro Blanco [samples DV 494-1Snee and DV 494-2Snee], Cerros Mamá e Hija [DV 484 3Asnee and DV 484-3Bsnee; DeVries and Jud, 2018], Cerros Colorado [CC-T1b; Gariboldi et al., 2017], and Cerro Huaricangana [DV 510-1Snee; DeVries et al., 2021]). Stanton (2014) had refer to this ash horizon as the "*T9.3 tuff*" and suggested its use as a reference level for the successions from the northern EPB. In the Sacaco sub-basin, two ash samples of reasonably similar age (9.37 ± 0.10 Ma) have also been identified (at El Jahuay [Alto Grande, sample 1; Muizon and Bellon, 1986], Aguada de Lomas [MG-63], see Table 1). Furthermore, a population of nine zircon crystal of this age was also identified at Yauca Road Cut [MG3-54]; see Fig. 4B). We consider the *T9.3 tuff* of

Stanton (2014) as a regional volcanic event that can be traced basin-wide, and so it can be used as a (relatively) synchronous and effectively correlatable stratigraphic level.

The youngest defined Pisco allosequence of the EPB, the P2, was deposited from ~8.4 Ma up to at least 6.71 Ma (see Fig. 2; Di Celma et al., 2018; Bosio et al., 2019). In the Sacaco sub-basin, coeval rocks to the P2 allosequence partly occur at Aguada de Lomas and Montemar. Establishing whether those successions correspond with the P2 is challenging given the highly fragmented outcrops of the Sacaco area, which makes it difficult to determine the continuity of sedimentary successions, as well as the sedimentary response to eustatic-driven sea-level changes. Hence, it is unclear whether the intraformational unconformity occurring between the upper Montemar and the lower Sud-Sacaco West succession does correspond with the erosive surface existing at the top of the P2 allosequence in the northern EPB.

Sedimentary successions from the Pisco Formation younger than ~6.7 Ma crop out at the Pisco, Ica, and Nazca Valleys (e.g., Macharé, 1987; Macharé and Fourtanier, 1987; Dunbar and Baker, 1988; DeVries, 1998; Brand et al., 2011; Esperante et al., 2015; DeVries and Jud, 2018; DeVries et al., 2021), but they have not been associated with any allosequence. Existing biostratigraphic and radiometric data indicate that Mio-Pliocene rocks from the Cerro Vildoso (upper Aguada de Lomas), Sud-Sacaco West, Sacaco Chacra, and Yauca Depressions localities (6.3–4.5 Ma) are correlatable in part with those occurring at Cerro Blanco, Cerro Caucato, Cerro Huaracangana, Cerro Tiza, Cerro la Virgen, Monte de Queso, and Puente Huamaní (Mertz, 1966; Macharé, 1987; Macharé and Fourtanier, 1987; Dunbar and Baker, 1988; Marty, 1989; DeVries, 1998; O'Hare, 2015; Esperante et al., 2015; DeVries and Jud, 2018; Solis, 2018; DeVries et al., 2021). Likewise, the new radiometric results from the Caracoles Formation indicate that it was deposited during the latest Pliocene-early Pleistocene (2.7 Ma up to at least 1.9 Ma; Ochoa et al., 2021). It is thus time-equivalent to the late Pliocene-Pleistocene Changuillo Formation exposed to the north, close to the Nazca River (14.8°S; Macharé, 1987; Montoya et al., 1994). The Changuillo Formation includes siltstones, (tuffaceous) sandstones, and conglomerates with occurrences of balanid barnacles and bivalve shells, and has been described as a marine-continental transitional formation (Montoya et al., 1994; DeVries, 1998), indicating similar sedimentary environments to those from the Caracoles Formation. The Pongo Formation, the youngest marine unit of the Sacaco sub-basin (DeVries, 2020), was deposited during the early Pleistocene (around 1.4 Ma; Table 1). This unit, although representing different depositional environments, is time-equivalent to the Cañete Formation, which crops out from the Cañete River Valley (Fernández, 1993; Salazar, 1993) to the northern part of the EPB (right flank of the Pisco River; Petersen, 1954).

5.4. Source dynamics based on zircon-population age patterns

The youngest component of the detrital-zircon spectra in the Sacaco sedimentary record (23–~1.2 Ma) are derived from volcanic activity associated with the Neo-Quaternary Andean orogeny (18-4 Ma; Sébrier et al., 1998; Jaillard et al., 2000; Wipf, 2006). This signature could form after some andesitic volcanism associated with magmatic arcs such as the Huaylillas-Calipuy Arc (24-10 Ma; Mamani et al., 2010) and the Barroso inferior-Negritos Arc (10-3 Ma; Mamani et al., 2010) or from the erosion of proximal autochthonous volcano-sedimentary deposits occurring within the Chilcatay (21-17 Ma [Di Celma et al., 2018; Bosio et al., 2020]/?17-14 Ma [DeVries et al., 2021]) and Pisco (14.8-?2.5 Ma; Macharé and Fourtanier, 1987; Solis, 2018; Bosio et al., 2020) formations. This Neo-Quaternary signature also dominates modern samples from both the Ica River and the extrabasinal Ocoña River (Fig. 5; Pepper et al., 2016), indicating the active erosion of the Neogene magmatic arcs, as well as the Pisco and Chilcatay formations at present time. Zircon morphologies do not show particular size trends allowing further provenance discrimination (see Fig. S3 in Appendix B). The presence of Plio-Pleistocene marine terrace deposits (and associated molluscan content) at Quebrada Gramonal supports a substantial erosional topography carved in Pisco and Chilcatay beds as early as the Pliocene.

A late Cretaceous (100-65 Ma) and a late Jurassic-early Cretaceous (160-125 Ma) detrital-zircon populations are recorded within the Sacaco record. Zircons with late Cretaceous ages (100-65 Ma) are consistently present in the Sacaco area since the late Miocene, with a population slightly less abundant than the early Cretaceous one. Sources for late Cretaceous zircon signature are associated with a regional emplacement of the Coastal Batholith Complex (102-59 Ma; Mukasa, 1986; Wipf, 2006; Prudhomme et al., 2019). Present-day river samples show a markedly abundant zircon population of late Cretaceous age (Fig. 5; Pepper et al., 2016). Considering that the Coastal Batholith extends across the EPB, affecting the catchment areas of modern and ancient rivers, such differences in abundance indicate would either a re-emergence of the older source areas, a reactivation of the erosion of older areas or their sedimentary derived rocks, or a recent increase in the erosive processes affecting the Coastal Batholith.

The late Jurassic-early Cretaceous (160-125 Ma) signature exhibits similar crystallization ages to those associated with Jurassic to early Cretaceous igneous rocks (Mukasa, 1986; Clark et al., 1990; Vidal et al., 1990) associated to the magmatic arcs of the Rio Grande and Casma (145-105 Ma; Mamani et al., 2010; Ccallo et al., 2013). These arcs would be formed under an extensive phase affecting the South American continental margin during late Jurassic-early Cretaceous times, and which promoted the formation of relatively igneous bodies at intra-arc settings (Ramos, 2008). The late Jurassic-early Cretaceous zircon population seems to most closely match the ages reported for the Torconta Super-unit, which has been ascribed to the Casma magmatic arc (Rodriguez et al., 2012; Santos et al., 2014). This zircon population is continuously present in the Sacaco record from 10 Ma but shows a decrease in abundance towards the present, probably related with the progressive increase of the Neo-Quaternary signature after the Andean surficial uplift (Fig. 5).

The oldest zircon population is of early Neoproterozoic age (850-735 Ma) and represents a somewhat enigmatic component. Zircon populations of similar age were previously reported from the Central Peruvian Andes (Chew et al., 2007; Mišković et al., 2009), and were recently associated with a Neoproterozoic granitoids from the Eastern Cordillera of Peru (Mišković et al., 2009). These granitoids were emplaced after the Grenville-Sunsás orogeny along the western margin of ancestral South America under a phase of extensional tectonics during the proto-Iapetus rifting of Rodinia (Chew et al., 2008; Mišković et al., 2009). Whether these Neoproterozoic granitoids are the only possible primary source of this zircon population is open to debate. However, those are the only known potential source rocks matching the detrital-zircon age populations that occur within the sediment's dispersal path. It is also possible that pre-Miocene rocks had provide recycled zircons of Neoproterozoic age. This Neoproterozoic signature is only found in rocks from the Pisco Formation dated between 10 and 6 Ma. No significant populations were found in successions younger than 6 My or within the modern river samples (Fig. 5; Pepper et al., 2016). Considering that there is not grain-size fractionation or substantial lithological changes within rocks of the Pisco Formation deposited around 6 My, the change in zircon population cannot be attributed to variations within the depositional environments. Hence, the disappearance of the Neoproterozoic population from the younger than 6-My record can be related either to a tectonic-forced relief change driving the formation of paleo-reliefs or to sediment source exhaustion.

Zircon crystals associated with the Precambrian Arequipa Massif (see Complejo Basal de la Costa in Fig. 1A), with affinities to the Mesoproterozoic Grenvillian orogeny (Chew et al., 2007; Loewy et al., 2004), are almost absent from the Sacaco sedimentary record (Fig. 5). Although some Mesoproterozoic grains were recovered from the present-day sediments (Pepper et al., 2016). Likewise, few zircons of Paleoproterozoic age (older than 2 Ga) indicate the presence of recycled sediments from different provinces from the Amazon Craton (e.g., Tassinari et al.,

2000).

5.5. Tectono-sedimentary evolution of the Sacaco sub-basin

The EPB is an elongated basin that progressively becomes shallower towards the south (15°S) as the Coastal Cordillera shoals (Outer Shelf High in Thornburg and Kulm, 1981; Whitsett, 1976). The Sacaco sub-basin likely would have been formed as a perched depocenter in response to this shoaling during the late Miocene. However, whether it was completely isolated from the EPB remains to be investigated. Existing chronostratigraphic controls indicate that inner to middle-shelf deposits started to accumulate into a continually subsiding Sacaco sub-basin during Tortonian times (around 10–9.6 Ma, Fig. 8), while experiencing active syndepositional volcanism. Sedimentary successions correlative with the upper P1 allomember that crop out in the upper Ica River Valley (Di Celma et al., 2017; Bosio et al., 2019), also started to accumulate in the Sacaco sub-basin from 9.5 Ma onwards. Whether both sequences accumulated after the same transgressive event is still uncertain. Nonetheless, considering that during the middle to late Miocene (12-8 Ma) sea level was rather constant, with a slight tendency to a lowering of 20–30 m below present (Fig. 8; Miller et al., 2020), the onset of sedimentation across the EPB during the Tortonian must have occurred under a regime of marked tectonic subsidence (Schildgen et al., 2007). In the Sacaco sub-basin, the maximum flooding extent and greatest subsidence was reached towards the end of the late Miocene during the accumulation of the Pisco Formation and was controlled by a NW-SE fault system (Viveen and Schlunegger, 2018).

The last preserved rocks of the Pisco Formation correspond to immature gray medium-to-coarse sand beds, intercalating with bio-supported sandstones and shell banks containing, among others, bivalves, gastropods, barnacles, and coral reefs (see Yauca Depressions locality; Ochoa et al., 2021), accumulated at shallow water depths. The age of these successions (4.5 Ma; Ochoa et al., 2021) coincides with a progressive sea-level rise of ±20 m (Fig. 8; Miller et al., 2020). The regressive trend observed upwards in the Pisco Formation can be ascribed to a tectonic activity rather than to eustasy. This interpretation is also supported by the existence of a Pliocene angular and erosive unconformity existing between the Pisco and Caracoles formations (DeVries, 2020; Ochoa et al., 2021), and the last occurrences of warm-water and/or coastal Pisco-related taxa, such as the aquatic sloth *Thalassocnus*, the walrus-like dolphin *Odobenocetops*, and the gavialoid *Piscogavialis* (Ochoa et al., 2021), which indicate a strong disruption of coastal-marine habitats during the early Pliocene (from 4.5 to 2.7 Ma).

Following the Pliocene angular unconformity, sedimentation was reactivated at 2.7 Ma with the accumulation of shallow marine sediments of the Caracoles Formation. The Sacaco sub-basin appears to have undergone a reduction in the size of sedimentary depocenters in relation to those of the Pisco Formation. This reduction could also have been

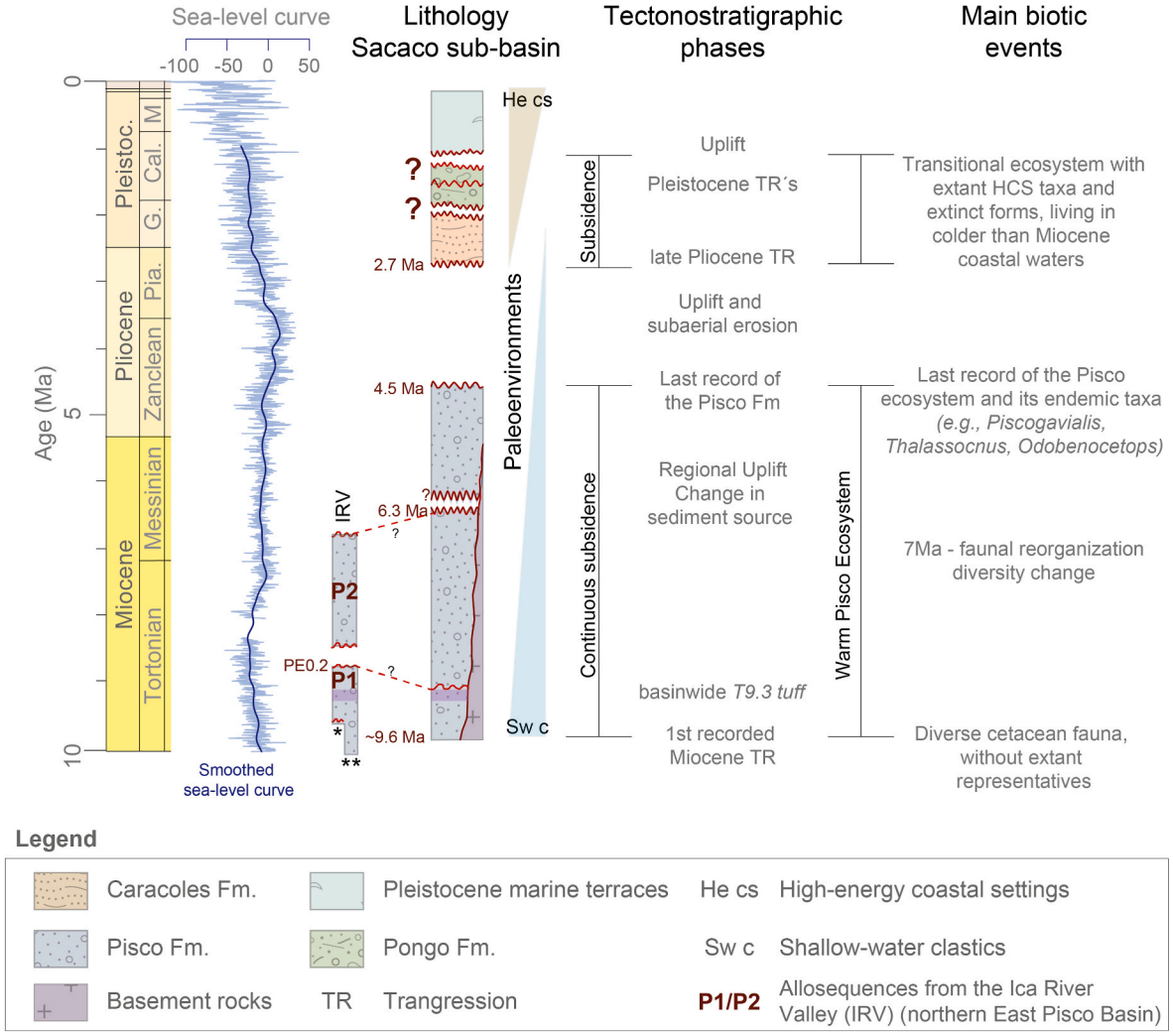

Fig. 8. Tectonostratigraphic evolution of the Sacaco sub-basin, indicating main tectonic phases and biotic events inferred for the Sacaco sub-basin and its relation with to the known chronostratigraphic frame from the Ica River Valley (IRV). Relative global sea level curve after Miller et al. (2020). *P1 age model according to Di Celma et al. (2017), 2018; Bosio et al. (2020), **P1 age model according to DeVries et al., 2021).

induced by a continuous 30-m eustatic fall experienced during the Pliocene (Fig. 8; Miller et al., 2020) and the increasing influence of the longshore-migrating axis of the Nazca Ridge (e.g., Hampel, 2002). Finally, the Pongo Formation accumulated in several sectors located near the present-day coastline (i.e., Aguada de Lomas, Quebrada Caracoles, and Quebrada Pongo as far south as Quebrada del Toro Muerto, the Río Acarí, the Acarí Depression, and the pampa landward of the Yauca Depressions), under a regime of obliquity-forced sea-level changes of 40–70 m (Miller et al., 2020). The Pongo and Intra-Pongo unconformities are then likely related to sea-level falls occurring between 1.9 and 1.4 Ma, likely between the MIS 50 and 46 (scenario 2 of DeVries, 2020). The vertebrate paleontological record from the Caracoles and Pongo formations shows a transitional community, containing taxa such as otariids (eared seals) and walruses (Ochoa et al., 2021) associated with cool waters and coastal upwelling. The structure of those coastal-marine faunas was likely shaped by a combination of factors including the Plio-Pleistocene global cooling trend and the reduction of neritic habitats after the last Andean uplift pulse and the obliquity-forced sea-level changes.

6. Conclusions

The combined used of radiogenic strontium isotopes, U–Pb geochronology and diatom-based biostratigraphy allowed us to assess depositional ages for the Mio-Pleistocene sedimentary rocks from the Sacaco sub-basin, and so a robust chronostratigraphic timeframe for this record was established. The Pisco Formation was found to range from ~9.6 to 4.5 Ma, the overlying Caracoles Formation from 2.7 to ~1.9 Ma, and the Pongo Formation from ~1.9 up to at least 1.4 Ma (Fig. 6). Six (tectonic or eustatic-driven) unconformities existing within this succession were further identified and time-constrained. The newly built chronostratigraphic framework is essential for correlating existing geological and paleontological data from physically disconnected localities so that a better picture of the Mio-Pleistocene evolution of the coastal-marine ecosystems can be drawn (Fig. 8).

The lithostratigraphic record provides evidence of a continually subsiding Sacaco sub-basin during Mio-Pleistocene times. This record shows a shallowing-upwards trend, indicating that maximum flooding extension and greatest subsidence was reached during the deposition of the Pisco Formation. Analysis of the sediment provenance based on zircon populations revealed an overall influence of mixed sources with discrete up-section changes in density. The Neo-Quaternary syndepositional volcanic Andean signature is conspicuously recorded in the Pisco, Caracoles, and Pongo formations, as well as the late Cretaceous signal related to the continuous erosion of the Coastal Batholith. By contrast, zircon populations associated with the early Cretaceous magmatic arcs gradually become less frequent within the Sacaco sedimentary record, likely in response to the Neogene uplifting. Finally, we also detected an early Neoproterozoic signal related to granitoid plutonism from the Grenville-Sunsás orogeny and the break-up of Rodinia, which vanishes from the sedimentary record by 6 Ma in response to either sediment source exhaustion or a large tectonic-induced paleogeographic change.

CRediT authorship contribution statement

Diana Ochoa: Formal analysis, Conceptualization, Funding acquisition, Methodology, Writing – original draft, Project administration, Writing – review & editing. **Thomas J. DeVries:** Conceptualization, Writing – original draft, Writing – review & editing. **Kelly Quispe:** Data curation, Formal analysis, Investigation, Writing – original draft. **Angel Barbosa-Espitia:** Methodology, Investigation, Formal analysis, Writing – original draft. **Rodolfo Salas-Gismondi:** Funding acquisition, Writing – original draft. **David A. Foster:** Writing – original draft, Supervision, Methodology. **Renzo Gonzales:** Data curation, Investigation, Methodology. **Sidoine Revillon:** Data curation, Investigation, Methodology. **Raul Berrospi:** Investigation, Data curation. **Luis Pairazamán:** Investigation, Data curation. **Jorge Cardich:** Funding acquisition, Investigation, Project administration. **Alexander Perez:** Investigation, Data curation. **Pedro Romero:** Data curation, Investigation. **Mario Urbina:** Methodology, Investigation, Data curation. **Matthieu Carré:** Conceptualization, Funding acquisition, Writing – original draft.

Declaration of competing interest

The authors declare that they have no known competing financial interests or personal relationships that could have appeared to influence the work reported in this paper.

Acknowledgments

We gratefully thank J. Barron (United States Geological Survey, Menlo Park, California, USA) for his assistance with diatom identification for samples from the Aguada de Lomas and Sud-Sacaco West Localities. This research was partly supported by CONCYTEC- FONDECYT (Peru) through the *Programa de incorporación de investigadores* (Grant Nº E038-2019-02-FONDECYT-BM and Grant Nº 007-2017-FONDECYT). Main research funds were available through the CONCYTEC-FONDECYT research grant 105-2018 awarded to DO. We specially thank A. Altamirano (MHN-UMNSM, Peru) for logistical assistance during field campaigns (especially his careful inspection of Bella Union's old route). Two anonymous reviewers are gratefully acknowledged for their comments that helped improving this manuscript.

Appendix A. Supplementary data

Supplementary data to this article can be found online at https://doi.org/10.1016/j.jsames.2022.103799.

References

Adams, G.I., 1908. An Outline Review of the Geology of Peru, Annual Report. Smithosonian Institution, Washington, pp. 385–430.
Adams, J., 1906. Caudal, procedencia y distribución de aguas de los Dptos. de Lima e Ica. Bol. Cuerpo Ing. 5, 367–379.
Barron, J.A., 2003. Planktonic marine diatom record of the past 18 my: appearances and extinctions in the Pacific and Southern Oceans. Diatom Res. 18 (2), 203–224.
Bosio, G., Malinverno, E., Collareta, A., Di Celma, C., Gioncada, A., Parente, M., Berra, F., Marx, F.G., Vertino, A., Urbina, M., 2020. Strontium isotope stratigraphy and the thermophilic fossil fauna from the middle Miocene of the east Pisco Basin (Peru). J. S. Am. Earth Sci. 97, 102399. https://doi.org/10.1016/j.jsames.2019.102399.
Bosio, G., Malinverno, E., Villa, I., Di Celma, C., Gariboldi, K., Gioncada, A., Barberini, V., Urbina, M., Bianucci, G., 2019. Tephrochronology and chronostratigraphy of the Miocene Chilcatay and Pisco formations (East Pisco basin, Peru). Newsl. Stratigr. 53 (2), 213–247. https://doi.org/10.1127/NOS%2F2019%2F0525.
Brand, L., Urbina, M., Chadwick, A., DeVries, T.J., Esperante, R., 2011. A high resolution stratigraphic framework for the remarkable fossil cetacean assemblage of the Miocene/Pliocene Pisco Formation, Peru. J. S. Am. Earth Sci. 31 (4), 414–425. https://doi.org/10.1016/j.jsames.2011.02.015.
Caldas, J., 1978. Geología de los Cuadrángulos de San Juan. Acarí y Yauca (Hojas 31-m. Ingemmet, Lima, Peru, 31-n 32-n).
Cardona, A., Cordani, U., Ruiz, J., Valencia, V., Armstrong, R., Chew, D., Nutman, A., Sanchez, A., 2009. U-Pb zircon geochronology and Nd isotopic signatures of the pre-Mesozoic metamorphic basement of the eastern Peruvian Andes: growth and provenance of a late Neoproterozoic to Carboniferous accretionary orogen on the northwest margin of Gondwana. J. Geol. 117 (3), 285–305.
Ccallo, W., Mamani, M., Acosta, H., Rodriguez, J., Cutipa, M., 2013. Petrogénesis de las rocas intrusivas del Grupo Casma (145--105 Ma) en el segmento Acarí-San Juan de Marcona. Bol. Soc. Geol. Peru 107, 22–26.
Chew, D., Kirkland, C., Schaltegger, U., Goodhue, R., 2007. Neoproterozoic glaciation in the Proto-Andes: tectonic implications and global correlation. Geology 35 (12), 1095–1098.
Chew, D.M., Magna, T., Kirkland, C.L., Mišković, A., Cardona, A., Spikings, R., Schaltegger, U., 2008. Detrital zircon fingerprint of the Proto-Andes: evidence for a Neoproterozoic active margin? Precambrian Res. 167 (1–2), 186–200.
Clark, A.H., Farrar, E., Kontak, D.J., Langridge, R.J., Arenas F, M.J., France, L.J., McBride, S.L., Woodman, P.L., Wasteneys, H.A., Sandeman, H.A., 1990. Geologic and geochronologic constraints on the metallogenic evolution of the Andes of southeastern Peru. Econ. Geol. 85 (7), 1520–1583.
Colbert, E.H., 1944. A New Fossil Whale from the Miocene of Peru, vol. 83. American Museum of Natural History, p. 32.

DeVries, T.J., 1998. Oligocene deposition and cenozoic sequence boundaries in the Pisco Basin (Peru). J. S. Am. Earth Sci. 11 (3), 217–231. https://doi.org/10.1016/S0895-9811(98)00014-5.
DeVries, T.J., 2017. Eocene stratigraphy and depositional history near Puerto caballas (East Pisco basin, Peru). Bol. Soc. Geol. Peru 112, 39–52.
DeVries, T.J., 2020. Lithostratigraphy and biostratigraphy of Pliocene and Pleistocene marine deposits and age of the highest marine terrace from the Sacaco basin and its environs (southern Peru). Bol. Soc. Geol. Peru 114, 20–48.
DeVries, T.J., Barron, J.A., Urbina-Schmitt, M., Ochoa, D., Esperante, R., Snee, L.W., et al., 2021. J.A., , M., , D., Esperante, The Miocene stratigraphy of the Laberinto area (Río Ica Valley) and its bearing on the geological history of the East Pisco Basin (south-central Peru). J. S. Am. Earth Sci. 111, 103458 https://doi.org/10.1016/j.jsames.2021.103458.
DeVries, T.J., Jud, N., 2018. Lithofacies patterns and paleogeography of the Miocene Chilcatay and lower Pisco depositional sequences (East Pisco basin, Peru). Bolet. Soc. Geol. Perú, Vol. Jubilar 8, 124–167.
Di Celma, C., Malinverno, E., Bosio, G., Collareta, A., Gariboldi, K., Gioncada, A., Molli, G., Basso, D., Varas-Malca, R.M., Pierantoni, P.P., 2017. Sequence stratigraphy and paleontology of the upper Miocene Pisco Formation along the western side of the lower Ica valley (Ica desert, Peru). Riv. Ital. Paleontol. Stratigr. 123, 255–273. https://doi.org/10.13130/2039-4942/8373.
Di Celma, C., Malinverno, E., Bosio, G., Gariboldi, K., Collareta, A., Gioncada, A., Landini, W., Pierantoni, P.P., Bianucci, G., 2018. Intraformational unconformities as a record of late Miocene eustatic falls of sea level in the Pisco Formation (southern Peru). J. Maps 14 (2), 607–619.
Di Celma, C., Malinverno, E., Cantalamessa, G., Gioncada, A., Bosio, G., Villa, I.M., Gariboldi, K., Rustichelli, A., Pierantoni, P., Landini, W., 2016a. Stratigraphic framework of the late Miocene Pisco Formation at cerro los quesos (Ica desert, Peru). J. Maps 12 (5), 1020–1028. https://doi.org/10.1080/17445647.2015.1115783.
Di Celma, C., Malinverno, E., Gariboldi, K., Gioncada, A., Rustichelli, A., Pierantoni, P., Landini, W., Bosio, G., Tinelli, C., Bianucci, G., 2016b. Stratigraphic framework of the late Miocene to Pliocene Pisco Formation at cerro Colorado (Ica desert, Peru). J. Maps 12 (3), 515–529. https://doi.org/10.1080/17445647.2015.1047906.
Dunbar, R., Baker, P., 1988. Cenozoic Geology of the Pisco Basin: Field Guidebook Regional IGCP. Genesis of Cenozoic Phophorites and Associated Organic-Rich Sediments: Peruvian Continental Margin, vol. 156. IGCP, Lima, Perú.
Dunbar, R.B., Marty, R.C., Baker, P.A., 1990. Cenozoic marine sedimentation in the Sechura and Pisco basins, Peru. Palaeogeogr. Palaeoclimatol. Palaeoecol. 77 (3), 235–261. https://doi.org/10.1016/0031-0182(90)90179-B.
Ehret, D.J., Macfadden, B.J., Jones, D.S., DeVries, T.J., Foster, D.A., Salas-Gismondi, R., 2012. Origin of the white shark Carcharodon (lamniformes: lamnidae) based on recalibration of the upper Neogene Pisco Formation of Peru. Palaeontology 55 (6), 1139–1153. https://doi.org/10.1111/j.1475-4983.2012.01201.x.
Esperante, R., Brand, L.R., Chadwick, A.V., Poma, O., 2015. Taphonomy and paleoenvironmental conditions of deposition of fossil whales in the diatomaceous sediments of the Miocene/Pliocene Pisco Formation, southern Peru—a new fossil-lagerstätte. Palaeogeogr. Palaeoclimatol. Palaeoecol. 417, 337–370. https://doi.org/10.1016/j.palaeo.2014.09.029.
Fedorov, A., Brierley, C., Lawrence, K.T., Liu, Z., Dekens, P., Ravelo, A., 2013. Patterns and mechanisms of early Pliocene warmth. Nature 496 (7443), 43.
Fedorov, A.V., Dekens, P., McCarthy, M., Ravelo, A., DeMenocal, P., Barreiro, M., Pacanowski, R., Philander, S., 2006. The Pliocene paradox (mechanisms for a permanent El Niño). Science 312 (5779), 1485–1489.
Fernández, M., 1993. Geologia de los cuadrangulos de Pisco, Guadalupe, Punta Grande, Ica y Córdova. In: INGEMMET (Ed.), A47, Carta Geol. Nac. Ser. A47, Carta Geol. Nac. INGEMMET, Lima, Peru.
Gariboldi, K., Bosio, G., Malinverno, E., Gioncada, A., Di Celma, C., Villa, I.M., Urbina, M., Bianucci, G., 2017. Biostratigraphy, geochronology and sedimentation rates of the upper Miocene Pisco Formation at two important marine vertebrate fossil-bearing sites of southern Peru. Newsl. Stratigr. 50 (4), 417–444. https://doi.org/10.1127/nos/2017/0345.
Garreaud, R.D., Molina, A., Farias, M., 2010. Andean uplift, ocean cooling and Atacama hyperaridity: a climate modeling perspective. Earth Planet Sci. Lett. 292 (1–2), 39–50.
Hampel, A., 2002. The migration history of the Nazca Ridge along the Peruvian active margin: a re-evaluation. Earth Planet Sci. Lett. 203 (2), 665–679. https://doi.org/10.1016/S0012-821X(02)00859-2.
Horton, B.K., 2018. Tectonic regimes of the central and southern Andes: responses to variations in plate coupling during subduction. Tectonics 37 (2), 402–429.
INGEMMET, 2016. MAPA GEOLÓGICO DEL PERÚ Escala 1:1'000.000. Ingemmet, Lima, Peru.
INGEMMET, 2017. Mapas Geológicos 1:100,000. INGEMMET, Lima, Peru.
Jaillard, E., Hérail, G., Monfret, T., Díaz-Martínez, E., Baby, P., Lavenu, A., Dumont, J., 2000. Tectonic evolution of the Andes of Ecuador, Peru, Bolivia and northernmost Chile. In: Cordani, U., Milani, E., Thomas Fliho, A., Campos, D.A. (Eds.), Tectonic Evolution of South America. Sociedade Brasileira de Geologia, Rio Janeiro, pp. 481–559.
Lambert, O., Muizon, C.d., 2013. A new long-snouted species of the Miocene pontoporiid dolphin Brachydelphis and a review of the Mio-Pliocene marine mammal levels in the Sacaco Basin, Peru. J. Vertebr. Paleontol. 33 (3), 709–721. https://doi.org/10.1080/02724634.2013.743405.
León, W.R., Rosell, W., Alemán, A.M., Torres, V.R., De la Cruz Matos, O., 2008. Estratigrafía, sedimentología y evolución tectónica de la cuenca Pisco Oriental. Bolet. INGEMMET, Ser. D 27, 1–154 (Lima, Peru).
Lisson, C., 1925. Algunos fósiles del Peru. Bol. Soc. Geol. Peru 23–30.
Loewy, S.L., Connelly, J.N., Dalziel, I.W., 2004. An orphaned basement block: the Arequipa-Antofalla Basement of the central Andean margin of South America. Geol. Soc. Am. Bull. 116 (1–2), 171–187.
Ludwig, K., 2003. User's Manual for IsoPlot 3.0. A Geochronological Toolkit for Microsoft Excel, p. 71.
Macharé, J., 1987. La Marge Continentale du Pérou: Régimes Tectoniques et Sédimentaires Cénozoiques de L'avant-Arc des Andes Centrales. PhD Thesis, Universite de Paris Sud, Paris, France, p. 391.
Macharé, J., Fourtanier, E., 1987. Datations des formations tertiaires du bassin de Pisco (Pérou) à partir d'associations de diatomées. Comptes rendus de l'Académie des sciences. Sér. 2, Méc. Phys. Chim. Sci. l'uni. Sci. Terre 305 (5), 407–412.
Macharé, J., Ortlieb, L., 1992. Plio-Quaternary vertical motions and the subduction of the Nazca Ridge, central coast of Peru. Tectonophysics 205 (1–3), 97–108. https://doi.org/10.1016/0040-1951(92)90420-B.
Mamani, M., Navarro, P., Carlotto, V., Acosta, H., Rodriguez, J., Jaimes, F., Santos, A., Rodríguez, R., Chavez, L., Cueva, E., Cereceda, C., 2010. Arcos magmaticos Meso-Cenozoicos del Perú, XV Congreso Peruano de Geología. Sociedad Geológica del Perú, Cusco, Peru, pp. 563–570.
Marocco, R., Muizon, C.d., 1988. Los vertebrados del Neogeno de la costa sur del Perú: ambiente sedimentario y condiciones de fosilización. Bullet. l'Inst. Fr. d'études Andines 17 (2), 105–117.
Marty, R.C., 1989. Stratigraphy and Chemical Sedimentology of Cenozoic Biogenic Sediments from the Pisco and Sechura Basins, Peru. Doctoral Thesis, Rice University, Houston, Texas, p. 301.
McArthur, J., Howarth, R., Bailey, T., 2001. Strontium isotope stratigraphy: LOWESS Version 3: best fit to the marine Sr-isotope curve for 0-509 Ma and accompanying look-up table for deriving numerical age. J. Geol. 109, 155–170. https://doi.org/10.1086/319243.
McArthur, J., Howarth, R., Shields, G., 2012. Strontium isotope stratigraphy. Geol. Time Scale 1, 127–144. https://doi.org/10.1016/B978-0-444-59425-9.00007-X.
Mertz, D., 1966. Mikropaläontologische und sedimentologische Untersuchungen der Piscoformation Südperus. Palaeontograph. Abteilung B 1–51.
Miller, K.G., Browning, J.V., Schmelz, W.J., Kopp, R.E., Mountain, G.S., Wright, J.D., 2020. Cenozoic sea-level and cryospheric evolution from deep-sea geochemical and continental margin records. Sci. Adv. 6 (20), eaaz1346.
Mišković, A, et al., 2005. Carboniferous plutonism along the Eastern Peruvian Cordillera: Implications for the Late Paleozoic to Early Mesozoic Gondwanan tectonics. 6th International Symposium on Andean Geodynamics (ISAG 2005, Barcelona, Extended Abstracts), 508–511.
Mišković, A., Spikings, R.A., Chew, D.M., Košler, J., Ulianov, A., Schaltegger, U., 2009. Tectonomagmatic evolution of Western Amazonia: geochemical characterization and zircon U-Pb geochronologic constraints from the Peruvian Eastern Cordilleran granitoids. Geol. Soc. Am. Bull. 121 (9–10), 1298–1324.
Montoya, M., García, W., Caldas, J., 1994. Geologia de los cuadrangulos de Lomitas, Palpa, Nasca y Puquio; Hojas: 30-l, 30-m, 30-n y 30-ñ. In: INGEMMET (Ed.), A53, Carta Geol. Nac. Ser. A53, Carta Geol. Nac. INGEMMET, Lima, Peru.
Muizon, C.d., Bellon, H., 1980. L'âge mio-pliocène de la Formation Pisco (Pérou). Comptes Rendus de l'Académie des Sciences de Paris, pp. 1063–1066.
Muizon, C.d., Bellon, H., 1986. Nouvelles données sur l'âge de la Formation Pisco (Pérou). Comptes rendus de l'Académie des sciences. Sér. 2, Méc. Phys. Chim. Sci. l'uni. Sci. Terre 303 (15), 1401–1404.
Muizon, C.d., DeVries, T.J., 1985. Geology and paleontology of late Cenozoic marine deposits in the Sacaco area (Peru). Geol. Rundsch. 74 (3), 547–563. https://doi.org/10.1007/BF01821211.
Muizon, C.d., Mcdonald, H.G., Salas-Gismondi, R., Urbina, M., 2003. A new early species of the aquatic sloth Thalassocnus (Mammalia, Xenarthra) from the Late Miocene of Peru. J. Vertebr. Paleontol. 23 (4), 886–894. https://doi.org/10.1671/2361-13.
Muizon, C.d., McDonald, H.G., Salas-Gismondi, R., Urbina, M., 2004. The youngest species of the aquatic sloth Thalassocnus and a reassessment of the relationships of the nothrothere sloths (Mammalia: Xenarthra). J. Vertebr. Paleontol. 24 (2), 387–397. https://doi.org/10.1671/2429a.
Mukasa, S.B., 1986. Zircon U-Pb ages of super-units in the Coastal batholith, Peru: implications for magmatic and tectonic processes. Geol. Soc. Am. Bull. 97 (2), 241–254.
O'Hare, D.J., 2015. High-Resolution Correlation of a Time-Bounded Unit of the Pisco Formation, Peru. Master Thesis, Loma Linda University, Electronic Theses, Dissertations & Projects, p. 170. Paper 333.
Ochoa, D., Salas-Gismondi, R., DeVries, T.J., Baby, P., Altamirano-Sierra, A., Barbosa, A., Foster, D.A., Urbina-Schmitt, M., Quispe, K., Cardich, J., Gutiérrez, D., Perez-Segovia, A., Valqui, J., Carré, M., 2021. Late Neogene evolution of the Peruvian margin and its ecosystems: a synthesis from the Sacaco record. Int. J. Earth Sci. https://doi.org/10.1007/s00531-021-02003-1.
Pepper, M., Gehrels, G., Pullen, A., Ibanez-Mejia, M., Ward, K.M., Kapp, P., 2016. Magmatic history and crustal genesis of western South America: constraints from U-Pb ages and Hf isotopes of detrital zircons in modern rivers. Geosphere 12 (5), 1532–1555.
Petersen, G., 1954. Informe preliminar sobre la geología de la faja costanera del Departamento de Ica. Bolet. Técn. Empres. Petrol. Fisc. 1, 33–41.
Pilleri, G., Siber, H., 1989. Neuer spättertiärer cetotherid (Cetacea, Mysticeti) aus der Pisco Formation Perus. Beiträge Paläontol. Cetaceen Perus 1, 108–122.
Pin, C., Santos-Zalduegui, J., 1997. Sequential separation of light rare-earth elements, thorium and uranium by miniaturized extraction chromatography: application to isotopic analyses of silicate rocks. Anal. Chim. Acta 339 (1–2), 79–89.
Prudhomme, A., Baby, P., Robert, A., Brichau, S., Cuipa, E., Eude, A., Calderon, Y., O'Sullivan, P., 2019. Western Thrusting and Uplift in Northern Central Andes (Western Peruvian Margin), Andean Tectonics. Elsevier, pp. 299–331.

Ramos, V.A., 2008. The basement of the Central Andes: the Arequipa and related terranes. Annu. Rev. Earth Planet Sci. 36, 289–324.
Rech, J.A., Currie, B.S., Jordan, T.E., Riquelme, R., Lehmann, S.B., Kirk-Lawlor, N.E., Li, S., Gooley, J.T., 2019. Massive middle Miocene gypsic paleosols in the Atacama desert and the formation of the central andean rain-shadow. Earth Planet Sci. Lett. 506, 184–194.
Rodriguez, J., Acosta, H., Cutipa, M., Ccallo, W., Mamani, M., 2012. Petrogénesis del Cretácico inferior y metamorfismo del Cretácico superior en el sur de Perú: La super unidad Torconta, XVI Congreso Peruano de Geología. Sociedad Geológica del Perú, Lima, Peru, p. 5.
Salazar, H., 1993. Geologia de los cuadrangulos de Mala, Lunahuaná, Tupe, Conayca, Chincha, Tantará y Castrovirreyna, A44, Carta Geol. Nac. Ser. A44, Carta Geol. Nac. INGEMMET, Lima, Peru.
Santos, A., Weimin, G., Soberon, D., Torres, D., Ccallo, W., 2014. Magmatismo y litogeoquímica de los granitoides del Jurásico y Cretácico entre Chala y Atico. Bol. Soc. Geol. Peru 109, 1–6.
Schildgen, T.F., Hodges, K.V., Whipple, K.X., Reiners, P.W., Pringle, M.S., 2007. Uplift of the western margin of the Andean plateau revealed from canyon incision history, southern Peru. Geology 35 (6), 523–526.
Sébrier, M., et al., 1988. Tectonics and uplift in Central Andes (Peru, Bolivia and northern Chile) from Eocene to present. Géodynamique 3 (1–2), 85–106.
Solis, F., 2018. Bioestratigrafía e implicancias paleoceanográfica de las diatomeas de la sección Cerro Caucato, Formación Pisco, Ica, Perú. Master Thesis. Universidad Peruana Cayetano Heredia, Lima, Peru, p. 125.
Stanton, C., 2014. Correlation and Paleoenvironments above West T9. 3 Tuff, Pisco Formation, Peru. Master Thesis. Loma Linda University, p. 109.
Steinmann, G., 1904. Observaciones de Lima a Chanchamayo. Cuerpo Ing. Minas 12, 1–27.
Steinmann, G., 1930. Geología del Perú. Heidelverg. Winters Universitätsbuchhandlung.
Tassinari, C.C.G., Bettencourt, J.S., Geraldes, M.C., Macambira, M.J.B., Lafon, J.M., 2000. The Amazon craton. In: Cordani, U., Milani, E.J., Thomaz Filho, A., Campos Neto, M.C. (Eds.), Tectonic Evolution of South America: 31st International Geological Congress, pp. 41–95. Rio de Janeiro, Brazil.
Thornburg, T., Kulm, L., 1981. Sedimentary Basins of the Peru Continental Margin: Structure, Stratigraphy, and Cenozoic Tectonics from 6 S to 16 S Latitude, vol. 154. Geological Society of America Memoir, pp. 393–422.
Thouret, J.-C., Wörner, G., Gunnell, Y., Singer, B., Zhang, X., Souriot, T., 2007. Geochronologic and stratigraphic constraints on canyon incision and Miocene uplift of the Central Andes in Peru. Earth Planet Sci. Lett. 263 (3–4), 151–166.
Varas-Malca, R., Salas-Gismondi, R., Ochoa, D., DeVries, T.J., 2019. Filling the Gap in the History of Otariid Seals from the Southeastern Pacific Ocean. North American Paleontological Convention (NAPC), Riverside, California.
Vermeesch, P., 2018. IsoplotR: a free and open toolbox for geochronology. Geosci. Front. 9 (5), 1479–1493. https://doi.org/10.1016/j.gsf.2018.04.001.
Vidal, C.E., Injoque-Espinoza, J., Sidder, G.B., Mukasa, S.B., 1990. Amphibolitic Cu-Fe skarn deposits in the central coast of Peru. Econ. Geol. 85 (7), 1447–1461.
Viveen, W., Schlunegger, F., 2018. Prolonged extension and subsidence of the Peruvian forearc during the Cenozoic. Tectonophysics 730, 48–62. https://doi.org/10.1016/j.tecto.2018.02.018.
Whitsett, R.M., 1976. Gravity Measurements and Their Structural Implications for the Continental Margin of Southern Peru. PhD Thesis, Oregon State University, USA, p. 82.
Wipf, M.A., 2006. Evolution of the Western Cordillera and Coastal Margin of Peru: Evidence from Low-Temperature Thermochronology and Geomorphology. ETH Zurich.